

TECHNICAL NOTE

D-1605

EXPLORATORY INVESTIGATION OF THE EFFECT OF A
FORWARD-FACING JET ON THE BOW SHOCK OF A BLUNT BODY IN
A MACH NUMBER 6 FREE STREAM

By David J. Romeo and James R. Sterrett

Langley Research Center
Langley Station, Hampton, Va.

NATIONAL AERONAUTICS AND SPACE ADMINISTRATION
WASHINGTON

February 1963

NATIONAL AERONAUTICS AND SPACE ADMINISTRATION

TECHNICAL NOTE D-1605

EXPLORATORY INVESTIGATION OF THE EFFECT OF A
FORWARD-FACING JET ON THE BOW SHOCK OF A BLUNT BODY IN
A MACH NUMBER 6 FREE STREAM

By David J. Romeo and James R. Sterrett

SUMMARY

The effect of a forward-facing jet on the bow shock of a blunt body in a Mach 6 free stream was investigated experimentally. The models tested had forward-facing jets using air and helium exhausting at Mach numbers from 1 to 10.3 and were run through a range of the ratio of jet total pressure to free-stream total pressure of 0.03 (jet off) to 2.5. The ratio of body diameter to jet-exit diameter varied from 1.12 to 55.6 and the angle of attack was varied from 0° to 35° .

The experimental results show that the main-stream shock can be affected by the jet in two significantly different ways. One way is simply to move the strong shock away from the body without altering its shape. The second and perhaps more interesting case occurs when the jet causes a large displacement of the main shock and considerably changes its shape. It was found that the ratio of jet total pressure to free-stream total pressure necessary to obtain the large displacements of the main-stream shock depended on the ratio of body diameter to jet-exit diameter and also on the jet-exit Mach number. The maximum amount the shock could be displaced in percent of body diameter was seen to increase with increasing jet-exit Mach number and also with decreasing ratio of body diameter to jet-exit diameter. For the models that were investigated through an angle-of-attack range, the displacement became very unsteady and fell off sharply as the angle of attack was increased.

Simplified theoretical considerations applied to the shock-displacement phenomena provide a possible explanation for the two different types of main-stream shock displacement. Theoretical curves show the regions where these types of displacement would occur for different exit Mach numbers and pressure ratios for a forward-facing jet in a Mach 6 stream.

INTRODUCTION

The idea of injecting a gas forward into a free-stream flow was explored as early as 1951 when some investigations were made (ref. 1) to see the effect of a forward-facing sonic jet on the drag of a blunt body in transonic flow. Other

investigations of forward-facing jet (refs. 2 to 6) have also been concerned mainly with the effect of the jet on the aerodynamic characteristics of the body from which they issued. Reference 4, for example, has shown that the pressure drag on a blunt body in supersonic flow can be significantly reduced by using a small forward-facing jet. Reference 5 illustrates the large effect that the ratio of jet total pressure to free-stream total pressure has on determining the shape of the bow shock over a blunt body when several jets or retrorockets are used.

At the present time a problem of great concern to the safe atmospheric reentry of space vehicles suggests another application of the forward-facing jet. Continuous-data transmission and communication contact of a reentering vehicle with the ground during a portion of its descent is lost because the strong shock that forms around the body raises the air temperature enough to ionize the gas which in turn prevents transmission of the radio signal. A gaseous jet should have the ability to some degree to cool the hot plasma and to induce recombination. In addition, it may, in some cases, greatly alter the shape and strength of the main-stream shock and thereby reduce the degree of ionization. Conceivably, an antenna extending from a reentering vehicle could use a gaseous jet issuing forward from its face as a means of allowing signal transmission.

In consideration of the above-mentioned areas of interest, the present investigation was undertaken because previous tests have not explored the use of jets with either high exhaust Mach numbers, or in a hypersonic main stream or over a wide range of ratios of body diameter to jet diameter. More specifically, the present paper presents the results of an investigation conducted to measure the penetration of a forward-facing jet and its effect on the main-stream shock wave in front of a blunt body in a Mach 6 free stream. The tests were conducted over a range of jet-exit Mach number, ratio of jet total pressure to free-stream total pressure, ratio of body diameter to jet-exit diameter, and angle of attack.

SYMBOLS

d_j	jet-exit diameter, in.
d_m	body diameter, in.
l	distance between foremost point of main-stream shock and model face, measured along model center line, in.
l_1	distance between initial intersection of jet mixing region and model face measured along model center line, in.
l_m	distance between a given center-line Mach number and face of model, measured along model center line, in.
p	pressure, lb/sq in. abs
M	Mach number

α	angle of attack measured between main-stream flow direction and model center line, deg
ν	Prandtl-Meyer turning angle, angle through which flow must expand from $M = 1.0$ to a given Mach number, deg
θ	angle between flow direction and model center line, deg
γ	ratio of specific heats

Subscripts:

∞	free-stream test-section conditions
j	jet conditions at exit, nominal value
t	stagnation condition
max	maximum
1	condition at jet nozzle just inside exit
2	condition at jet nozzle just outside exit

A prime mark denotes condition after a normal shock.

APPARATUS

This investigation was carried out in the Langley 20-inch Mach 6 tunnel. The tunnel is an intermittent type that exhausts to the atmosphere, and was operated at a stagnation pressure of approximately 365 pounds per square inch absolute for all tests with the exception of one in which the stagnation pressure was varied from 290 to 515 pounds per square inch absolute. The tunnel stagnation temperature was 400° F and the corresponding Reynolds number per foot was 6.9×10^6 for a stagnation pressure of 365 pounds per square inch absolute. A more complete description of the tunnel is presented in reference 7.

Models and Supports

The five basic models used in the tests were constructed of 1/2-inch-diameter stainless steel and were 8 inches long. In addition, three steel collars were constructed with outside diameters of 1, 2, and 3 inches. The collars were made to fit over and mount flush with the face of the models so as to yield body face diameters up to 3 inches. The five models and three collars are shown in figure 1(a). The apparent odd shape of the collars was due to the fact that the original plan was to make some tests with the collars reversed. The bodies are identified by two numbers; the first refers to the model used and the second to the collar. For example, body 23 would be model 2 with a 3-inch collar.

Some tests were made with helium to investigate exit Mach number effects. These tests were made with models without collars and the second number in this case ⁴ is used to designate the use of helium. (All other tests were made with air.) Since a fixed-nozzle area ratio will yield a different exit Mach number depending upon whether air or helium is used, the models are generally referred to by their model numbers. The nominal values of exit Mach number for air and helium for the bodies tested are given in figure 1(a) and are based upon one-dimensional area-ratio concepts.

Each model was supported by a 3/8-inch heavy-wall pipe and was mounted in the tunnel as shown in figure 1(b). To vary the angle of attack, the support was rotated in a horizontal plane. Because of the simplicity of the sting support, angular flow misalignment was in some cases as high as three quarters of a degree. The total pressure of the jet was measured by a pressure gage (0 to 1,000 pounds per square inch gage) connected to a 0.070-inch inside-diameter tube that was passed through the pipe into the settling chamber (large inside-diameter section before jet throat) of the model. The test gas was supplied to the model by means of the heavy-wall pipe which in turn was connected to either a 1,000-pound-per-square-inch-gage air supply or several 1,000-pound-per-square-inch-gage helium bottles. The chamber total pressure was controlled by a needle valve placed in the supply line and was monitored on the pressure gage. (The minimum or valve closed jet total pressure was the pressure behind a normal shock in the Mach 6 tunnel.)

Test Methods and Techniques

High-speed motion pictures and schlieren photographs were taken to record the flow phenomena. The motion pictures (400 frames per second) were taken for approximate durations of 5 to 7 seconds at representative test conditions and two to five schlieren photographs (exposure approximately 6×10^{-6} seconds) were taken at each test point. For reasons explained in the next section, the schlieren photographs rather than the movies were used to measure graphically the amount the jet flow displaced the main-stream shock, and therefore they constitute the basic data used in the program.

RESULTS AND DISCUSSION

Observed Shock Configurations

The high-speed movies showed that the alteration of the main-stream shock caused by the jet could be placed into two distinct categories. In the first category the alteration consisted of an increase in the size of the bow wave with no change in the general shape. This result is essentially the same as that which would have been obtained by increasing the size of the blunt body. In other words the main-stream flow appeared to see an increasingly large blunt-faced body as the jet pressure was increased. The bow shock in this case appeared to be quite steady. This category will herein be referred to as the strong-shock case. The second category observed in the movies was seen to be quite

different. The main stream shock was far removed from the face of the model. The shocks in this second category were seen to be unsteady in two different ways. In one way, the shock would tend to oscillate irregularly in a lateral direction but generally remain at the same axial location. In the other type of unsteadiness, the large shock displacement would "collapse" momentarily to the strong-shock case and then "pop out" or return to its position far ahead of the body. This second category will herein be referred to as the large-displacement case. The unsteadiness characterized by the lateral oscillations caused the movies to be unsatisfactory for graphically measuring the shock displacements; hence, the schlieren photographs were used for the data.

The movies, however, were very useful in analyzing the schlieren photographs and representations of all of the above-mentioned flow phenomena can be seen in the photographs of figures 2 to 6. An excellent illustration of the two cases of shock displacement can be seen in figure 4 for model 40, which has a nominal exit Mach number of 6.4 and a d_m/d_j of 1.12. The photos for $p_{t,j}/p_{t,\infty}$ of 1.10 to 2.51 show that the main-stream shock for this range is essentially of the same shape as a bow shock over a blunt body with no jet flow; this condition therefore is an example of the strong-shock case mentioned previously. The second case, the case of large displacements, is illustrated in the photographs of figure 4 for $p_{t,j}/p_{t,\infty}$ from 0.45 through 0.86. The photographs indicate that the main-stream shock is separated from the face of the model, by distances as great as 8 times that for the strong-shock case. The wavy appearance of the main-stream shock over the body illustrates the lateral oscillations or unsteadiness previously mentioned. The axial-flow unsteadiness is illustrated in figure 5 for model 50, which has a contoured nozzle and a nominal exit Mach number of 6.4 using air. At a pressure ratio $p_{t,j}/p_{t,\infty}$ equal to 1.55, both the large-displacement and the strong-shock cases can be seen. A much better description of the distinction between these two types of main-stream shock displacement will be given in the discussion of theoretical considerations.

Shock-Displacement Distances for the Two Types of Shock Configurations

The graphical determination of the main-stream displacement distances for the models which were tested are presented in figures 7 to 13 in terms of the measured shock-displacement distance divided by model diameter as a function of the ratio of jet total pressure to free-stream total pressure. The figures cover ranges of exit Mach number, model to jet-exit diameter ratio, and angle of attack.

Before looking at these data it will be very helpful to study figure 14 which is a sketch of the features used in interpreting the data. This figure is a general curve which can be used as a guide when mentally "fairing" the data of figures 7 to 13, in that it shows the region which has been called the large-displacement case. In some instances in the data, especially at the lower jet-exit Mach numbers, this region is not readily apparent. For example, in figure 7(a), which is for a sonic jet exit the region of large displacements is so small that the value of l_{max}/d_m as defined is actually smaller than the values

of l/d_m for the strong-shock case at high values of $p_{t,j}/p_{t,\infty}$. In figure 7(c) the region of large displacements was not reached with the pressure ratios available.

Comparison of the photographs of figures 2 to 6 and the corresponding data given in figures 7 to 13 shows that the pressure ratios necessary for the large-displacement case change considerably with exit Mach number and ratio of body diameter to jet diameter d_m/d_j . The pressure ratio for large displacements is seen to increase strongly with increasing jet exit Mach number and also with an increasing ratio of model diameter to jet-exit diameter. For example, for models 10 and 21 (figs. 7(a) and 8(b)) which have nominal exit Mach numbers of 1 and 3 and approximately equal diameter ratios, the maximum pressure ratios $p_{t,j}/p_{t,\infty}$ for large displacements are approximately 0.12 and 0.86, respectively. For models 20 and 31 (figs. 8(a) and 9(d)) which have nominal exit Mach numbers of 3 and 6.4 and which also have approximately equal diameter ratios, the values of $p_{t,j}/p_{t,\infty}$ for l_{max}/d_m are approximately 0.25 and 2.1, respectively. Comparing the diameter ratios for the same jet-exit Mach number (figs. 10(a) to 10(c), for example) shows that the pressure ratio $p_{t,j}/p_{t,\infty}$ for l_{max}/d_m increases from approximately 1.8 to 2.5 as the diameter ratio is increased from 1.12 to 4.48. For a diameter ratio of 6.76 (fig. 10(d)), the pressure ratio for l_{max}/d_m was not reached; thus, the range of test variables was not sufficient to obtain the pressure ratio for the large-displacement cases for all of the tests.

Figures 11 and 12 show the variation of l/d_m with $p_{t,j}/p_{t,\infty}$ as the angle of attack is increased from 0° to 35° . For both models l/d_m falls off rapidly for the large-displacement case and thus shows a strong dependence on angle of attack. Even an angle of attack as small as 2° causes a large reduction in the maximum values of l/d_m measured on model 50. (See figs. 12(a) and 12(b).) This reduction in l/d_m as the angle of attack is increased even slightly would tend to limit applicability of the large-displacement phenomena to practical uses only when extreme directional stability and very small angle-of-attack variation of the vehicle will be encountered. Because the measured sting misalignment in some cases was as high as three-quarters of a degree at a nominal zero-angle-of-attack setting, the question arises as to the possible inaccuracy in the quantitative values of l/d_m . A crude interpolation of the data of figure 12 which shows the angle-of-attack variation for model 50 indicates that a misalignment of three quarters of a degree could yield values of l/d_m that are low by as much as 20 percent. This error should not affect the qualitative discussion of the data that has been given but some caution must be used in comparing quantitative values. For example, the data for models 40 and 50, which have conical and contoured nozzles as their only difference, indicate that model 50 produces the larger values of l/d_m , but, since the values differ by only 30 percent, the data are not necessarily conclusive.

The runs made with helium (see figs. 6 and 13) were made without collars. The trends of l/d_m with $p_{t,j}/p_{t,\infty}$ are the same as with air except that no

maximum values of l/d_m were achieved for models 44 or 54. (See figs. 13(c) and 13(d).) As observed for the air-jet cases, the pressure ratio for l_{max}/d_m increases sharply as the exit Mach number is increased.

Figure 15 presents maximum values of l/d_m as a function of exit Mach number for both air and helium data. As indicated in the figure, in some cases it is not certain that a maximum value of l/d_m was reached. The data show that l_{max}/d_m increases greatly with jet exit Mach number for all the models tested. The plot also illustrates the decrease in l_{max}/d_m as d_m/d_j increases at a given Mach number. Since the figure includes both air and helium data, the trend of increasing l_{max}/d_m with increasing Mach number may not be a pure effect. Consideration of this problem will be given in the next section.

The ratio of jet total pressure to free-stream total pressure was varied for all but one of the tests by varying the jet total pressure. Figure 10(a) includes the results of the one test where the tunnel total pressure was varied. The overlap of the data for this model (model 50, $M_j = 6.4$ contoured) indicates that the main-stream shock-displacement distance was a function of the ratio of jet total pressure to free-stream total pressure rather than the jet pressure alone.

Theoretical Considerations

Theoretical model.— A complete theoretical solution of the shock-displacement problem would appear to be rather complex and will not be attempted in this paper. However, it is instructive to examine the simpler case of a two-dimensional jet exhausting into a counter-flow supersonic stream with various assumed boundary restrictions to provide an explanation of the two different types of observed main-stream shock displacement as well as to give some insight into the importance of the defining parameters.

Since the exterior static pressure at the lip of the nozzle of a forward-facing jet (region 2 in fig. 16) would apparently be affected by jet model geometry, jet total pressure, and so forth, various values of exit pressure were assumed in the subsequent analysis. For convenience, these pressures were expressed in terms of p_2/p_∞ and result in the following relationship:

$$\frac{p_1}{p_2} = \frac{p_1}{p_{t,j}} \frac{p_{t,\infty}}{p_\infty} \frac{p_\infty}{p_2} \frac{p_{t,j}}{p_{t,\infty}} \quad (1)$$

The static-pressure ratios at the end of the jet nozzle are thus dictated once values of $p_{t,j}/p_{t,\infty}$ and p_∞/p_2 are assumed for a given stream and jet-exit Mach number (the same static-pressure ratio at the end of the jet nozzle can be obtained by many combinations of $p_{t,j}/p_{t,\infty}$ and p_∞/p_2).

When a jet exhausts into still air or into an opposing stream, it undergoes compressions or expansions at the exit lip dependent upon whether p_1/p_2 is

less than or p_1/p_2 is greater than 1, respectively. These expansion or compression waves cross the jet and, if they meet the free boundary, are reflected as compression or expansion waves, respectively. (See, for example, refs. 8 and 9.) Along the jet boundary, a mixing zone exists between the flow external to the jet and that of the jet itself. In the absence of data concerning the mixing between opposing streams, it was assumed that the mixing zone penetrated the jet along a 3° line of action measured from the theoretical jet boundary. This value was assumed from the data of references 10 and 11 in which it appeared that the mixing boundary was not a strong function of Mach number.

Next, consider the flow in a very small stream tube on the center line of a forward-facing jet of the type that is shown in figure 16. In passing through normal shock waves, both flows become subsonic and must decelerate to equal stagnation pressures. (See also refs. 3 and 6.) The free-stream flow determines the value of this stagnation pressure and, in order for the jet nozzle flow to reach this value, it must reach a Mach number sufficient to allow the required total-pressure reduction through a normal shock. Thus,

$$p'_{t,j} = p'_{t,\infty} \quad (2)$$

or

$$\frac{p'_{t,j}}{p_{t,j}} = \frac{p'_{t,\infty}}{p_{t,\infty}} \frac{p_{t,\infty}}{p_{t,j}} \quad (2a)$$

where a prime mark denotes conditions after a normal shock. A somewhat similar type of flow could occur before a supersonic nozzle has started. The jet normal shock would occur within the nozzle and produce the required pressure loss. The flow leaving the nozzle would be subsonic.

Perfect gas flow being assumed, values for solving this equation can be obtained from compressible flow tables (for example, ref. 12) since $p'_{t,\infty}/p_{t,\infty}$ and $p'_{t,j}/p_{t,j}$ are functions of Mach number only.

Illustration of two types of shock displacement.- Coarse net characteristic diagrams for two-dimensional jets exhausting into still air at several different values of p_1/p_2 are sketched in figure 17. The exit static pressure for all drawings of figure 17 was assumed to be a constant ($p_2/p_\infty = 1.3$) and the total pressure of the jet was varied to produce different values of p_1/p_2 . Superimposed on the characteristic net is a 3° mixing boundary. In an actual case, the mixing region would affect the slope of the characteristic lines; however, these figures were drawn by assuming no interaction between the two.

It is instructive to examine the flow on the center line of figure 17 to see when a normal shock in the jet stream would produce stagnation pressures equal to the stagnation pressure behind a tunnel Mach number of 6 (in other

words, to examine the flow and determine when eq. (2a) would be satisfied for a given value of $p'_{t,\infty}/p_{t,\infty}$). For the compression case of figure 17(a), $p'_{t,j}$ is always greater than $p'_{t,\infty}$ in the region before the intersection of the mixing boundaries from the two sides. Because in this case the jet cannot expand to a Mach number high enough for $p'_{t,j}$ to be equal to $p'_{t,\infty}$ after a normal shock, it seems reasonable to assume that mixing from the sides must occur to dissipate some of the kinetic energy in the jet before the jet flow is terminated. This type of flow therefore corresponds to the large-displacement case. Similarly, the flow sketched in figures 17(b) and 17(c) would be classified as a large-displacement case since $p'_{t,j}$ is greater than $p'_{t,\infty}$ in the region before the mixing zones intersect. (An inspection of the schlieren photograph in fig. 18 shows expansion and compression waves similar to those drawn in fig. 17(c). Fig. 18 further indicates that several reflections of the waves have occurred before the jet flow is terminated.)

In figure 17(d), the flow on the center line has expanded sufficiently to reach a Mach number which will allow $p'_{t,j}$ to equal $p'_{t,\infty}$ before mixing boundaries overlap. Note that, if the supersonic jet flow terminates near the position where $p'_{t,j}$ equals $p'_{t,\infty}$ in figure 17(d), the shock-displacement distance would be much less than it is expected to be in figures 17(a), 17(b), and 17(c) where the supersonic jet flow can terminate only after a mixing interaction. The type of shock displacement for figure 17(d) therefore corresponds to the strong-shock case. Figure 19 illustrates the possible occurrence of a strong-shock case for a sonic nozzle exhausting into air with the termination boundary restriction that $p'_{t,j}$ would equal $p'_{t,\infty}$ for a tunnel Mach number of 6.00. Note that this strong-shock case occurs at relatively low values of $p_{t,j}/p_{t,\infty}$ compared with those of figure 17(d). This analysis, although not rigorous, does illustrate the occurrence of two different types of shock displacements which have been experimentally observed.

Regions of different types of shock displacement.— Figure 20 presents curves which show the regions where the two types of shock displacement would occur for different jet exit Mach numbers at various base static pressures. The solid line on this figure is the necessary jet flow Mach number for $p'_{t,j}$ to just equal $p'_{t,\infty}$ and is obtained from equation (2a) for M_∞ equal to 6.00. The dashed lines are the maximum possible jet Mach numbers obtained on the center line of the jet by expanding the jet air to the assumed base static pressures. These Mach numbers were calculated from equations (1) and the following equation:

$$v_{\max} = v_1 + 2(v_2 - v_1) \quad (3)$$

As is shown in figure 20, strong-shock cases would occur in the region above the intersection of the dashed and solid lines and large-displacement cases below the intersection. The dashed curves are begun at values that would give p_2/p_1 equal to 1; therefore, these curves do not indicate the pressures

where the large-displacement cases first occur. (However, the minimum pressure for large-displacement cases is apparently at least a function of the pressures necessary for starting a particular supersonic jet nozzle.) An inspection of the figures shows that the maximum $p_{t,j}/p_{t,\infty}$ for large-displacement cases at any given M_j increases as the base static pressure p_2/p_∞ increases. Since the experimental data have shown that increasing the collar size increases the maximum $p_{t,j}/p_{t,\infty}$ for large-displacement cases and theory indicated that as the base static pressure increases the maximum $p_{t,j}/p_{t,\infty}$ increases, the trends appear to be in agreement if it is reasoned that increasing the collar size increases the base static pressure. A comparison of equal base static-pressure lines ($p_2/p_\infty = \text{Constant}$) for different nozzle Mach numbers shows that the upper limit for large-displacement cases would terminate at lower values of $p_{t,j}/p_{t,\infty}$ when the nozzle Mach number is decreased. In fact, figure 20(a) shows that the large-displacement case would occur for a sonic jet nozzle only at relatively low total-pressure ratios. If the exit base static pressure p_2/p_∞ became as high as 50, which is greater than the static pressure behind a Mach 6 bow shock, the large-displacement cases would terminate at a $p_{t,j}/p_{t,\infty}$ of approximately 0.5. (This trend of decreasing maximum $p_{t,j}/p_{t,\infty}$ for large displacement with a decrease in nozzle exit Mach number was observed in the experimental data previously discussed.)

Figure 21 presents similar curves for helium jet nozzles exhausting into air. This figure indicates that changes in base static pressures p_2/p_∞ and nozzle exit Mach numbers for helium produce trends that are similar to those predicted for air. However, the maximum value of $p_{t,j}/p_{t,\infty}$ for a large-displacement case for helium can be quite different from that for air. For example, the maximum value of $p_{t,j}/p_{t,\infty}$ for a Mach 6 nozzle with base static pressures of p_2/p_∞ equal to 1.3 is 2.4 and 1.5, respectively, for air and helium. (Fig. 21(d) shows that a high Mach number helium nozzle would maintain large-displacement cases at relatively high values of total-pressure ratio; indications of this effect were observed in the previously discussed experimental data.)

Shock-displacement distances. - Order-of-magnitude estimates of shock-displacement distances can be made from the following considerations: (1) for the large-displacement cases the length of shock displacement would be greater than the distance l_1 from face of nozzle to interaction of mixing zones from the sides; (2) for strong-shock cases the length of shock displacement should be relatively close to the position l_m on the axis where the Mach number is sufficient to produce $p'_{t,j}$ equal to $p'_{t,\infty}$. These two parameters, l_1 and l_m , are plotted in figure 22 for a jet nozzle with M_j of 6.4 and were obtained by drawing several characteristic nets with mixing regions similar to that shown in

figure 17. By making use of figure 20 to determine which type of shock displacement would occur, figure 23 was plotted to show these distances as a function of $p_{t,j}/p_{t,\infty}$ for two values of exit static pressure. The lower limits of the curves in figure 23 were chosen so that the value of p_2/p_1 would be equal to 1.00. This condition would insure that the total pressure was sufficiently high for starting the supersonic jet nozzle; however, in an actual case, the nozzle would start before this condition was reached. In figure 23 the distance l_1 increases with increasing $p_{t,j}/p_{t,\infty}$ for a constant exit static pressure condition p_2/p_∞ until the strong-shock case occurs and the displacement drops to the l_m values shown. (As previously stated, the l_1 values are lower limiting values of the shock-displacement distances.) In an actual case, the exit static pressure may also vary with a change in $p_{t,j}/p_{t,\infty}$. Figure 23 indicates that the shock-displacement distance and type of shock configuration is very sensitive to the base static pressure p_2/p_∞ . Small changes in conditions could very well change the static pressures, cause rapid pattern changes, and result in observed instability for certain values of total pressures.

Also plotted in figure 23 is the experimentally observed shock-displacement distances obtained with model 50. A comparison of the data points and the computed curves shows that the data and theory agree in general magnitude.

CONCLUSIONS

An experimental investigation of the effect of a forward-facing jet on the bow shock of a blunt body in a Mach number 6 free stream led to the following conclusions:

1. The nature of the alteration of the main-stream shock caused by the jet could be placed into two distinct categories. In one case, the bow shock grew in size but retained its basic shape. In the second case the shock was far removed from the body and appeared to be less steady.
2. The cases corresponding to the large displacements occurred at higher values of total-pressure ratio either as the jet-exit Mach number or as the ratio of model diameter to jet-exit diameter was increased.
3. When the large-displacement case occurred, the length of the displacement with respect to the model diameter increased as the jet-exit Mach number was increased from 1 to 10.3, and also as the ratio of model diameter to jet-exit diameter was decreased and approached 1.0.
4. The large displacement of the main-stream shock was observed to fall off rapidly as the angle of attack was increased. This reduction in shock-displacement distance as the angle of attack is increased slightly would tend to

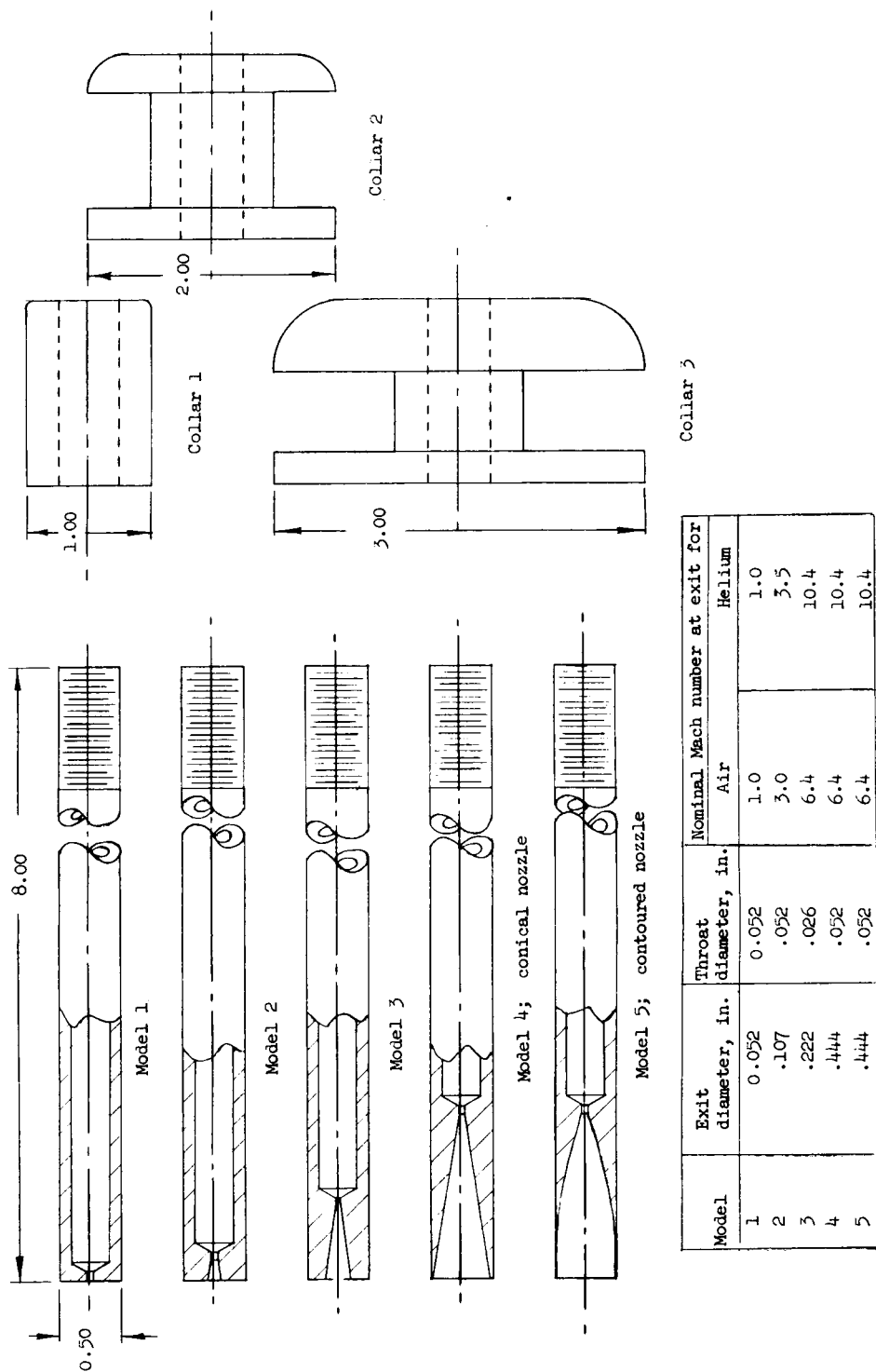
limit applicability of the large-displacement phenomena to vehicles with extreme directional stability and very small angle-of-attack variation over the flight range.

Simplified theoretical considerations provide a possible explanation for the two different types of main-stream shock displacement. For the small-shock standoff type of displacement, the flow on the center line for both the tunnel and jet have passed through normal shock waves. The flow issuing from the jet has expanded to a sufficiently high Mach number to allow a reduction of stagnation pressure through a normal shock which will balance the stagnation pressure of the tunnel flow behind the bow shock. For the large standoff shock case, the flow from the jet cannot expand sufficiently for this type of pressure balance, and a mixing process is required to reduce the jet kinetic energy before the jet flow can balance the stream stagnation pressure. Curves based on a two-dimensional analysis show the regions where the above-mentioned types of displacement would occur for different forward-facing jets with various exit Mach numbers and base static pressures in a Mach 6 stream. This type of analysis, although not rigorous, does predict trends observed experimentally and helps to clarify the mechanism by which the displacement takes place.

Langley Research Center,
National Aeronautics and Space Administration,
Langley Station, Hampton, Va., November 14, 1962.

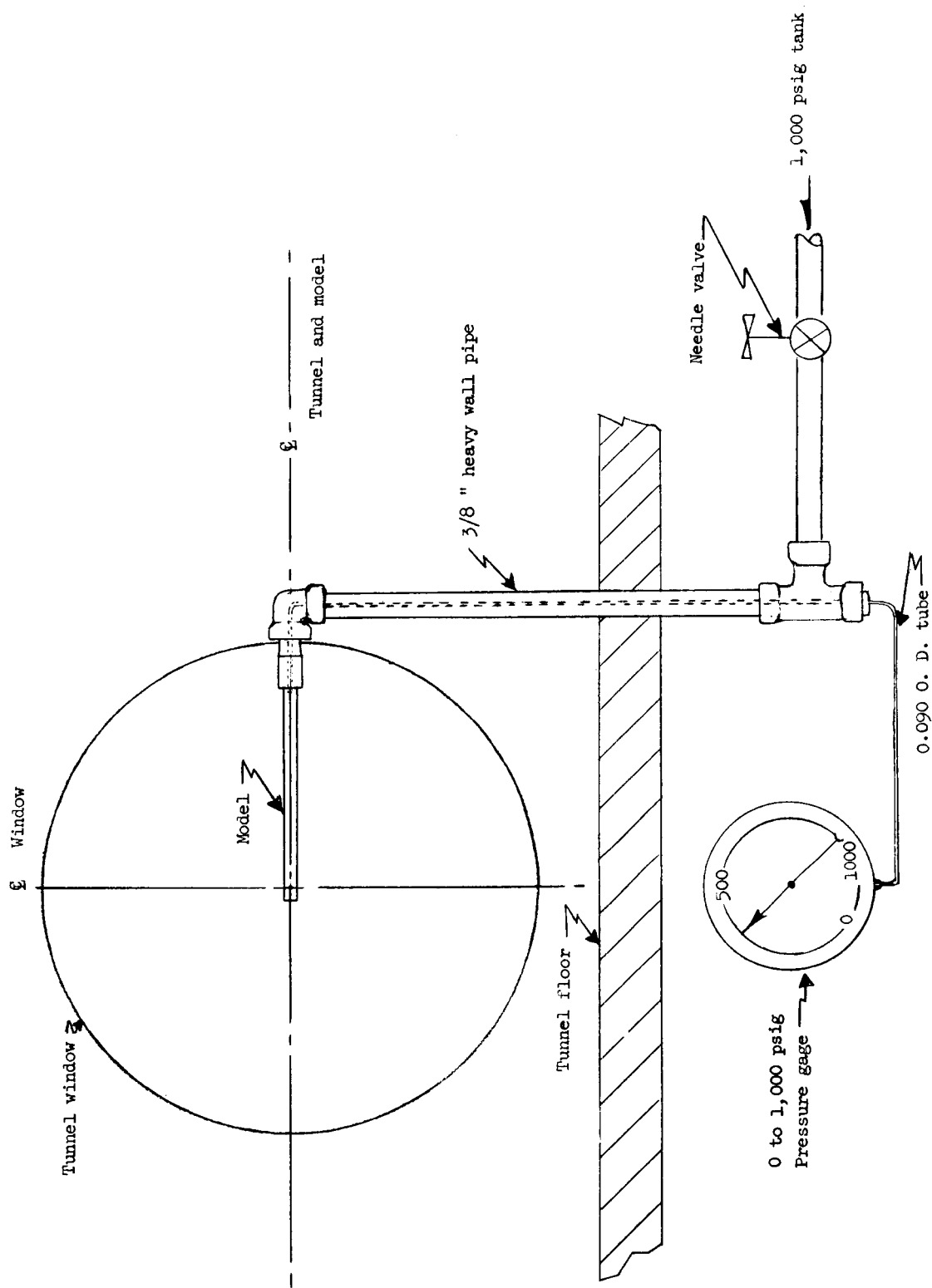
REFERENCES

1. Lopatoff, Mitchell: Wing-Flow Study of Pressure-Drag Reduction at Transonic Speed of Projecting a Jet of Air from the Nose of a Prolate Spheroid of Fineness Ratio 6. NACA RM L51E09, 1951.
2. Love, Eugene S.: The Effects of a Small Jet of Air Exhausting From the Nose of a Body of Revolution in Supersonic Flow. NACA RM L52I19a, 1952.
3. Hayman, Lovick O., Jr., and McDearmon, Russell W.: Jet Effects on Cylindrical Afterbodies Housing Sonic and Supersonic Nozzles Which Exhaust Against a Supersonic Stream at Angles of Attack From 90° to 180° . NASA TN D-1016, 1962.
4. Charczenko, Nickolai, and Hennessey, Katherine W.: Investigation of a Retro-rocket Exhausting From the Nose of a Blunt Body Into a Supersonic Free Stream. NASA TN D-751, 1961.
5. Peterson, Victor L., and McKenzie, Robert L.: Effects of Simulated Retro-rockets on the Aerodynamic Characteristics of a Body of Revolution at Mach Numbers From 0.25 to 1.90. NASA TN D-1300, 1962.
6. Watts, G. A.: An Experimental Investigation of a Sonic Jet Directed Upstream Against a Uniform Supersonic Flow. Tech. Note No. 7, Inst. Aerophys., Univ. of Toronto, Jan. 1956.
7. Sterrett, James R., and Emery, James C.: Extension of Boundary-Layer-Separation Criteria to a Mach Number of 6.5 by Utilizing Flat Plates With Forward-Facing Steps. NASA TN D-618, 1960.
8. Ferri, Antonio: Elements of Aerodynamics of Supersonic Flows. The Macmillan Co., 1949.
9. Love, Eugene S., Grigsby, Carl E., Lee, Louise P., and Woodling, Mildred J.: Experimental and Theroetical Studies of Axisymmetric Free Jets. NASA TR R-6, 1959. (Supersedes NACA RM L54L31 by Love and Grigsby, RM L55J14 by Love, RM L56G18 by Love, Woodling, and Lee, and TN 4195 by Love and Lee.)
10. Gooderum, Paul B., Wood, George P., and Brevoort, Maurice J.: Investigations With an Interferometer of the Turbulent Mixing of a Free Supersonic Jet. NACA Rep. 963, 1950. (Supersedes NACA TN 1857.)
11. Tollmien, Walter: Calculation of Turbulent Expansion Processes. NACA TM 1085, 1945.
12. Ames Research Staff: Equations, Tables, and Charts for Compressible Flow. NACA Rep. 1135, 1953. (Supersedes NACA TN 1428.)



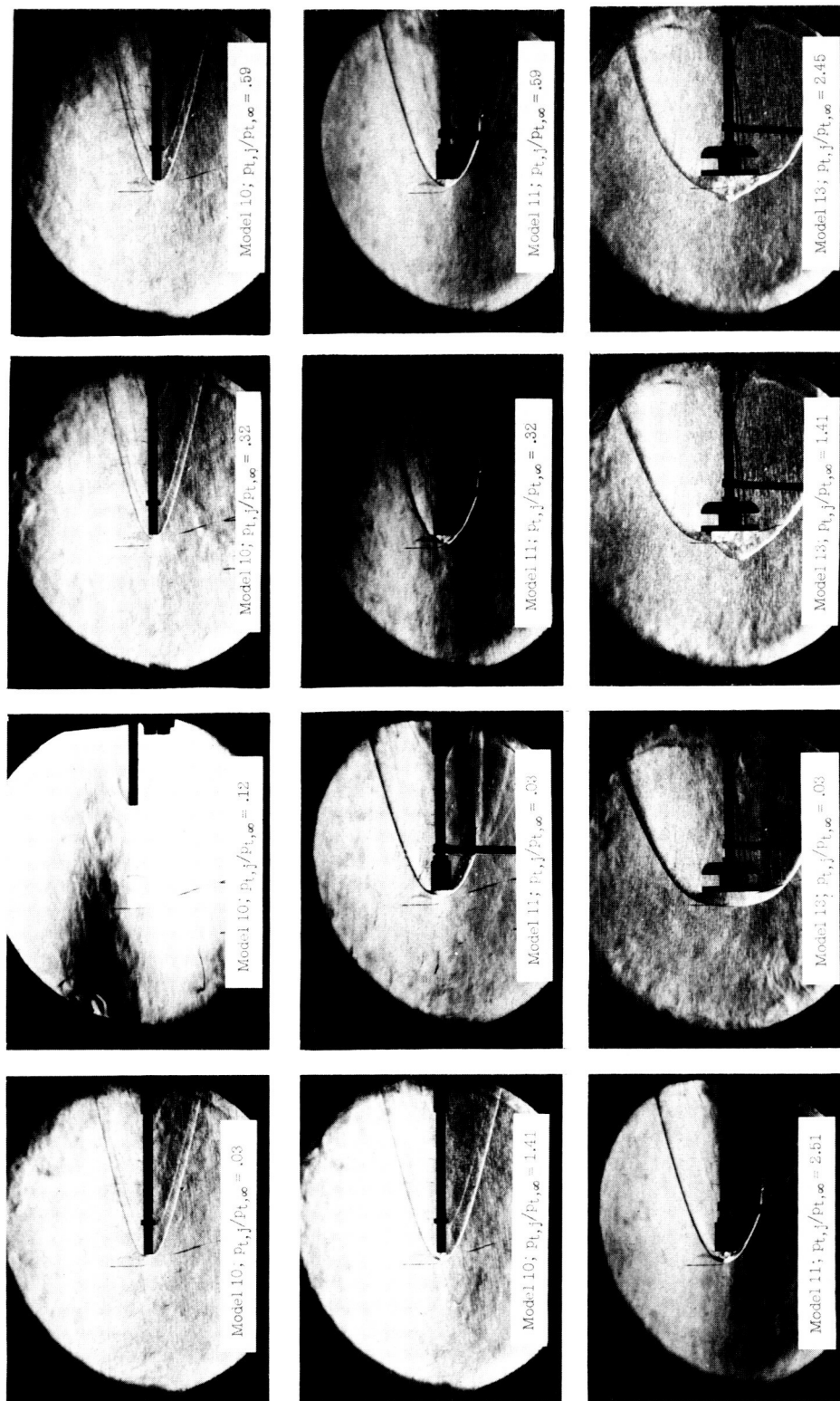
(a) Sketch of models and collars.

Figure 1.- Model description. All dimensions are in inches.



(b) Sketch of model mounted in tunnel.

Figure 1.- Concluded.



L-62-7035

Figure 2.- Schlieren photographs of the effects of the ratio of jet total pressure to free-stream total pressure and ratio of model diameter to jet diameter on main-stream shock-displacement distance for a nominal jet-exit Mach number of 1.0. $\alpha = 0^\circ$.

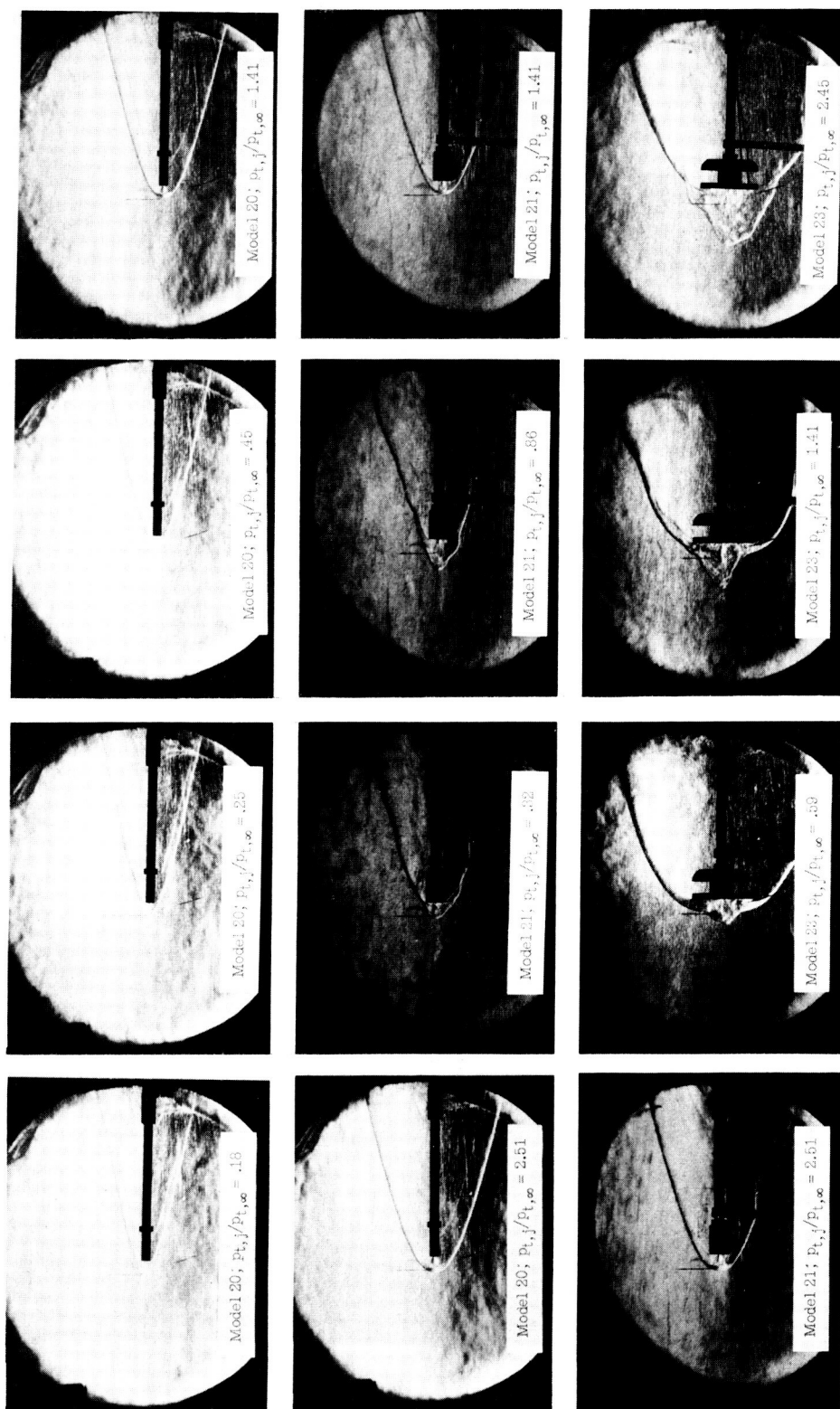
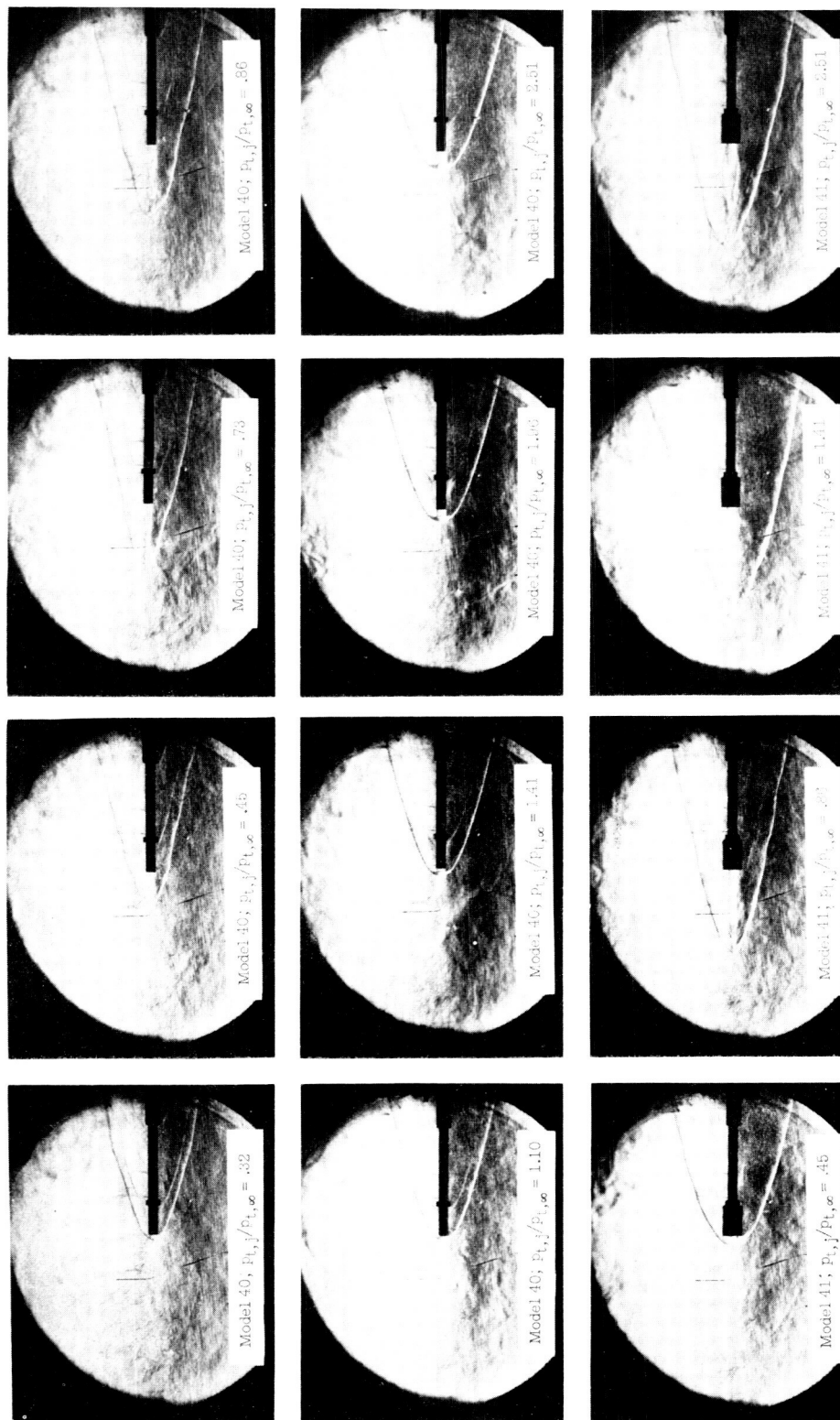


Figure 3.- Schlieren photographs of the effects of the ratio of jet total pressure to free-stream total pressure and ratio of model diameter to jet diameter on main-stream shock-displacement distance for a nominal jet-exit Mach number of 3.0. $\alpha = 0^\circ$.



L-62-7037

Figure 4.- Schlieren photographs of the effects of the ratio of jet total pressure to free-stream total pressure and ratio of model diameter to jet diameter on main-stream shock-displacement distance for a nominal jet-exit Mach number of 6.4. Conical nozzle; $\alpha = 0^\circ$.

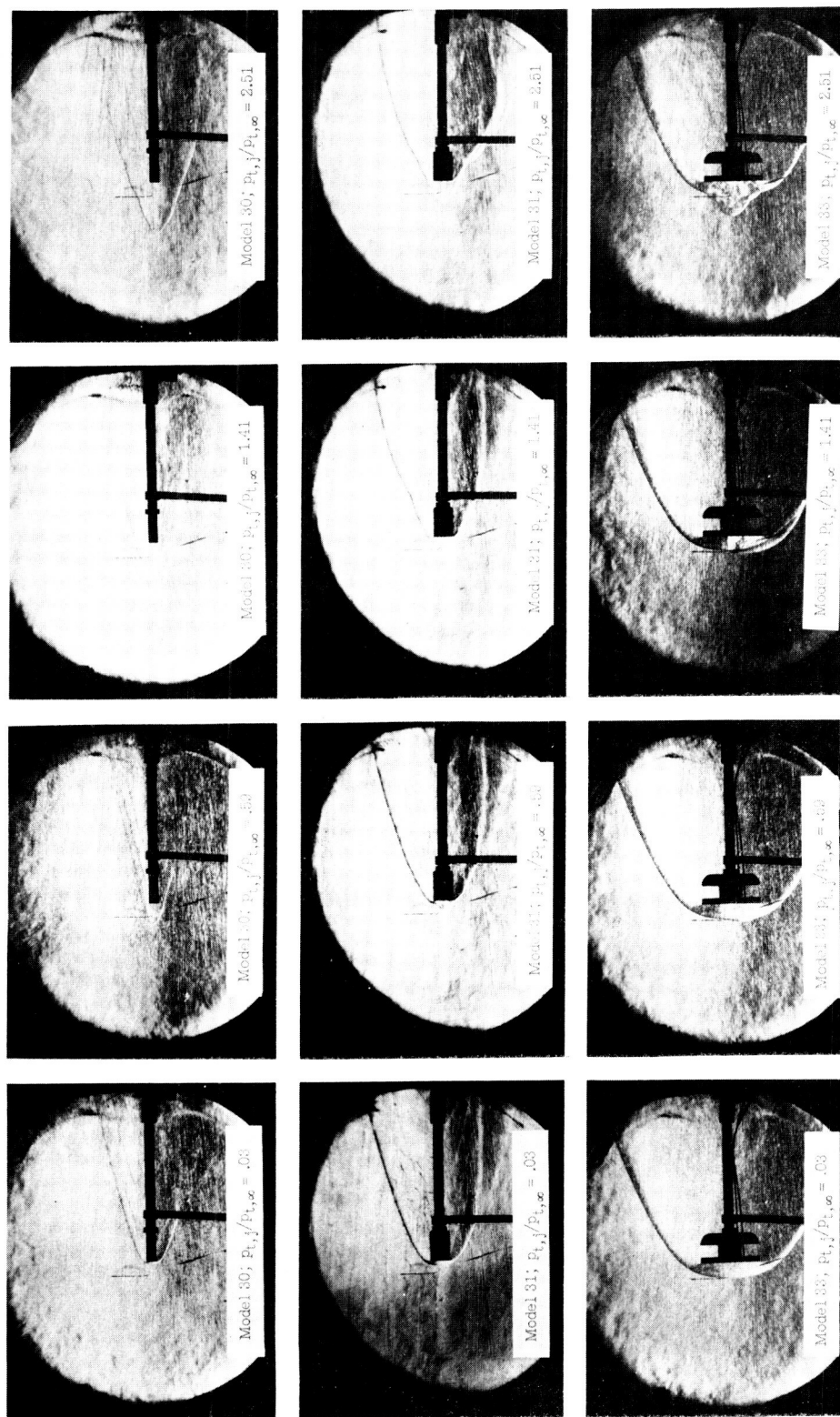
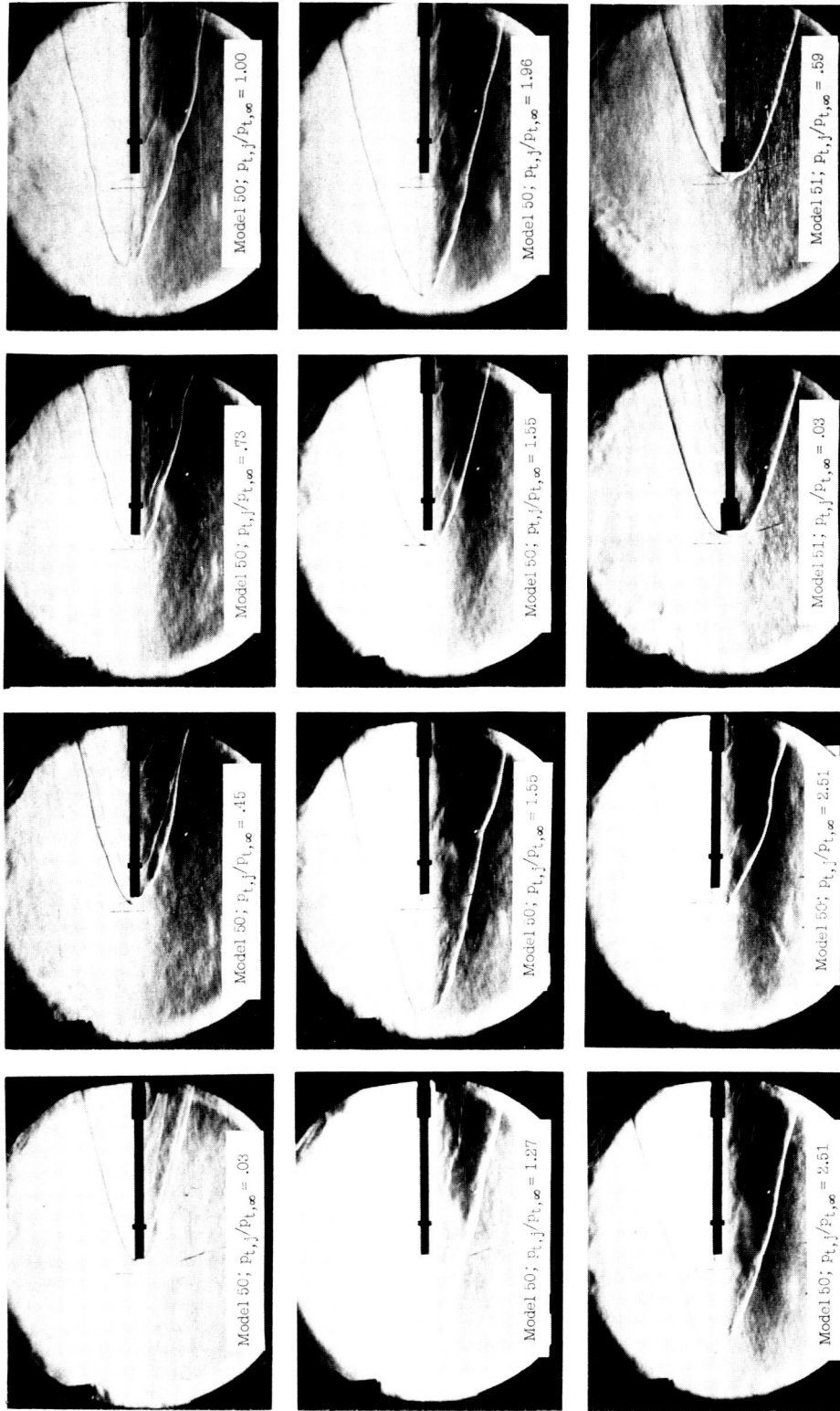


Figure 4.- Concluded. L-62-7038



L-62-7039

Figure 5.- Schlieren photographs of the effects of the ratio of jet total pressure to free-stream total pressure and ratio of model diameter to jet diameter on main-stream shock-displacement distance for a nominal jet-exit Mach number of 6.4. Contoured nozzle; $\alpha = 0^\circ$.

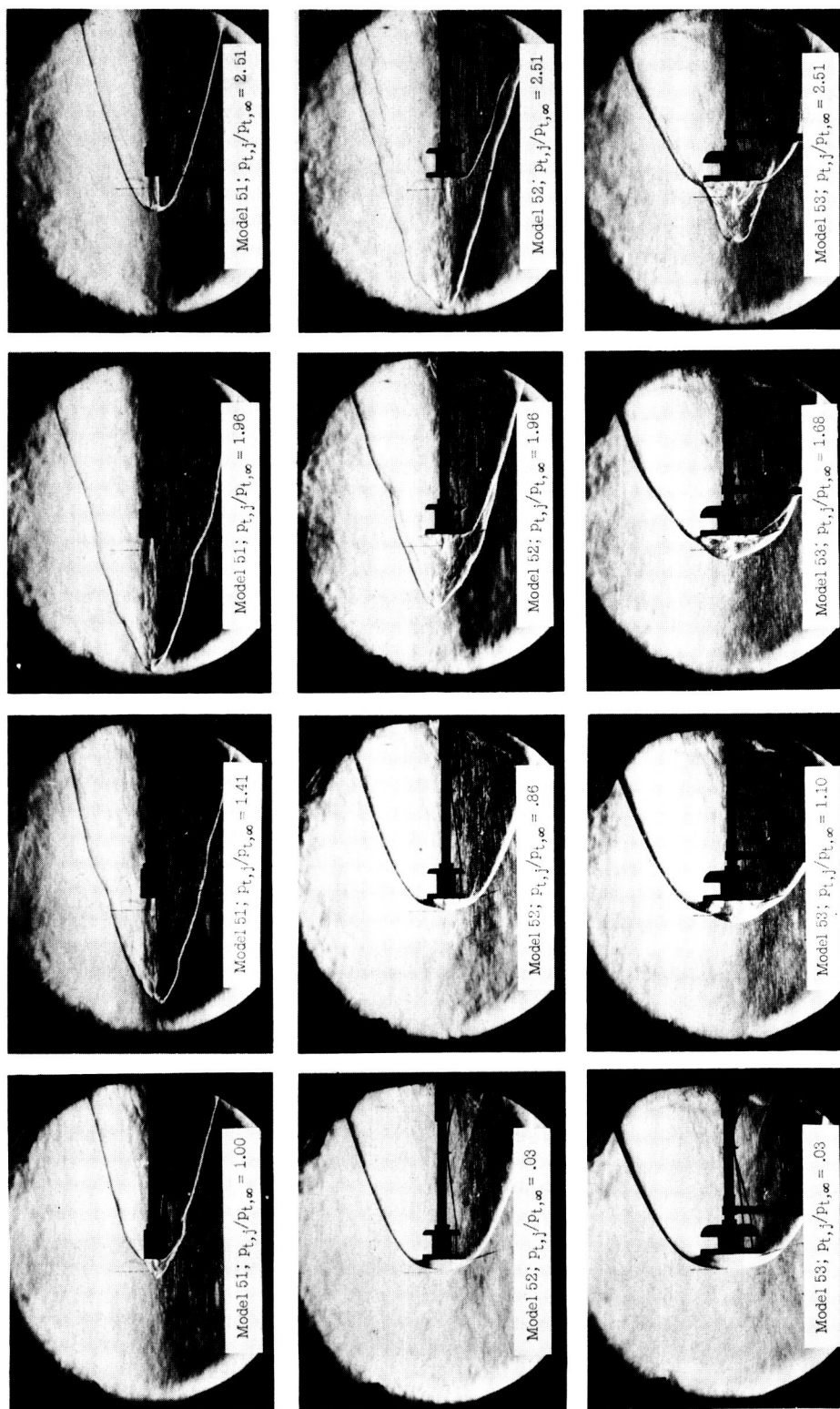


Figure 5.- Concluded. L-62-7040

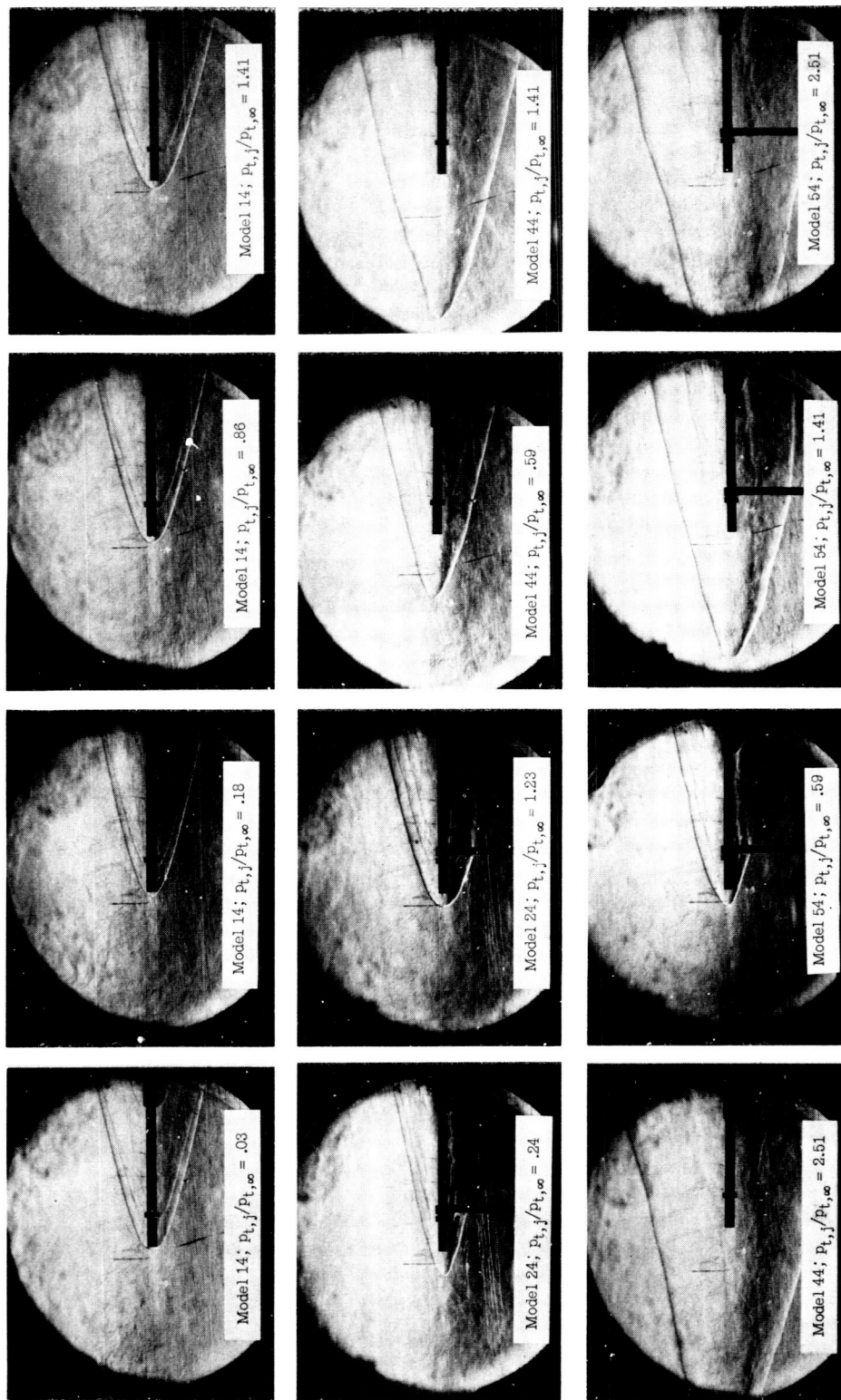
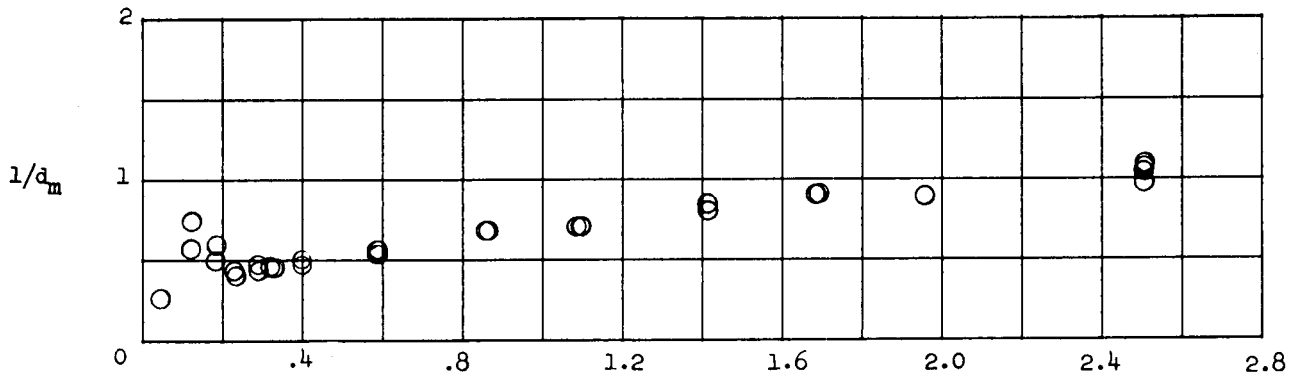
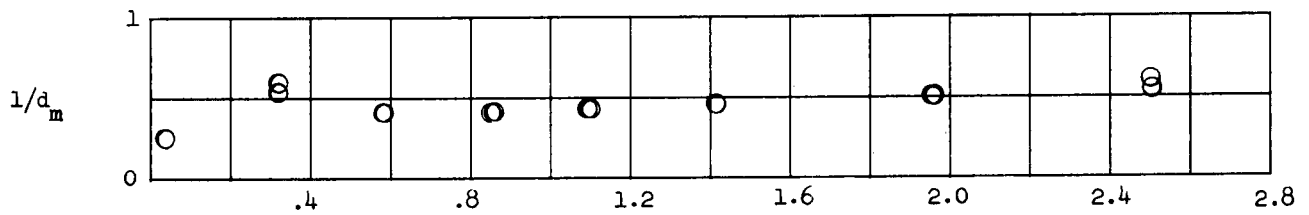


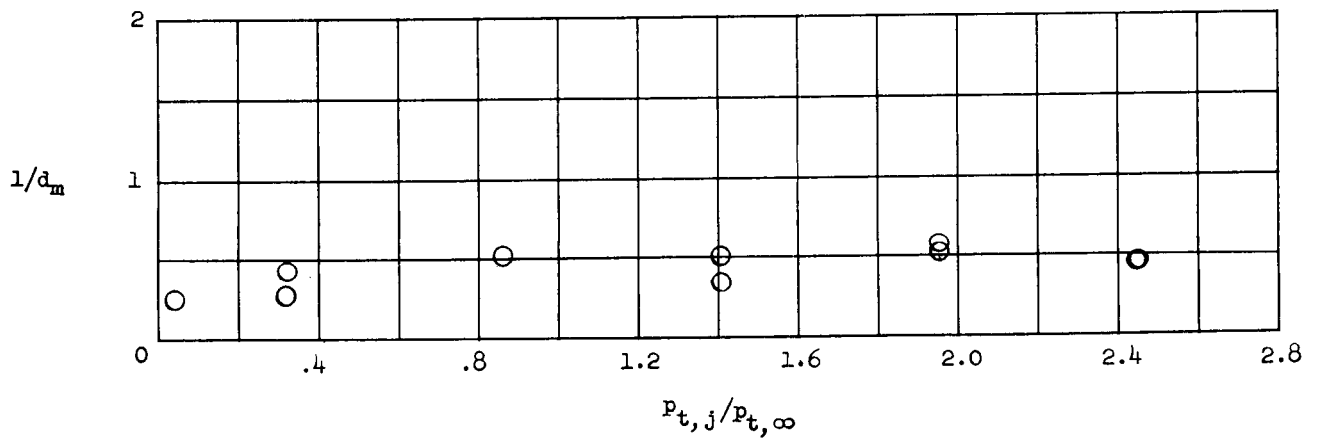
Figure 6.- Schlieren photographs of the effects of the ratio of jet total pressure to free-stream total pressure on main-stream shock-displacement distance for the tests which were conducted with helium. $\alpha = 0^\circ$.
L-62-7041



(a) Model 10; $d_m/d_j = 9.62$.

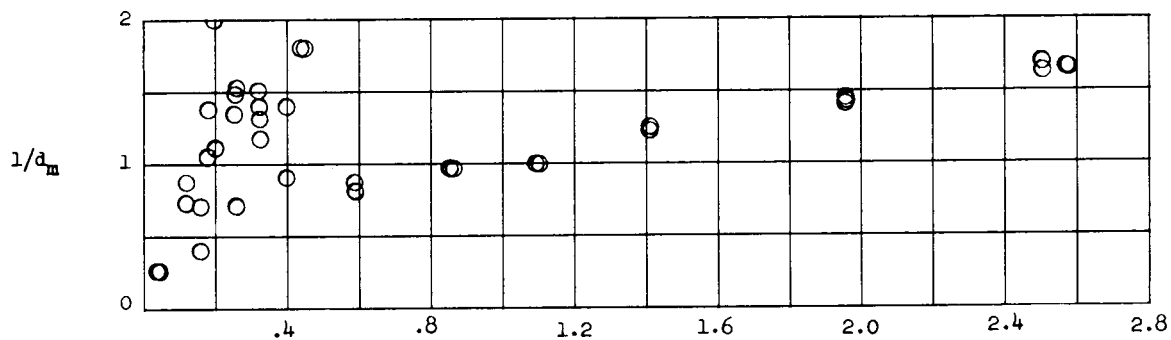


(b) Model 11; $d_m/d_j = 19.25$.

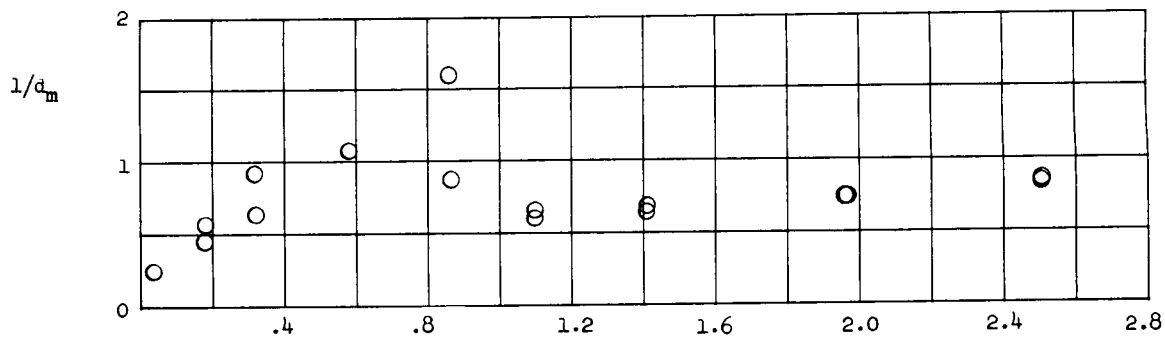


(c) Model 13; $d_m/d_j = 55.6$.

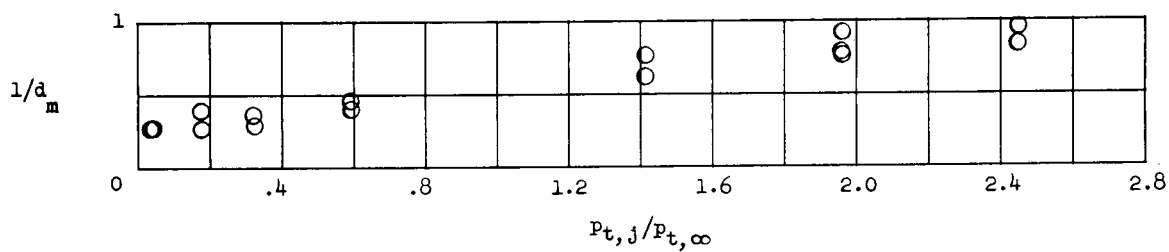
Figure 7.- Effect of ratio of jet total pressure to free-stream total pressure on main-stream shock-displacement distance for a nominal jet-exit Mach number of 1.0. $\alpha = 0^\circ$.



(a) Model 20; $d_m/d_j = 4.68$.

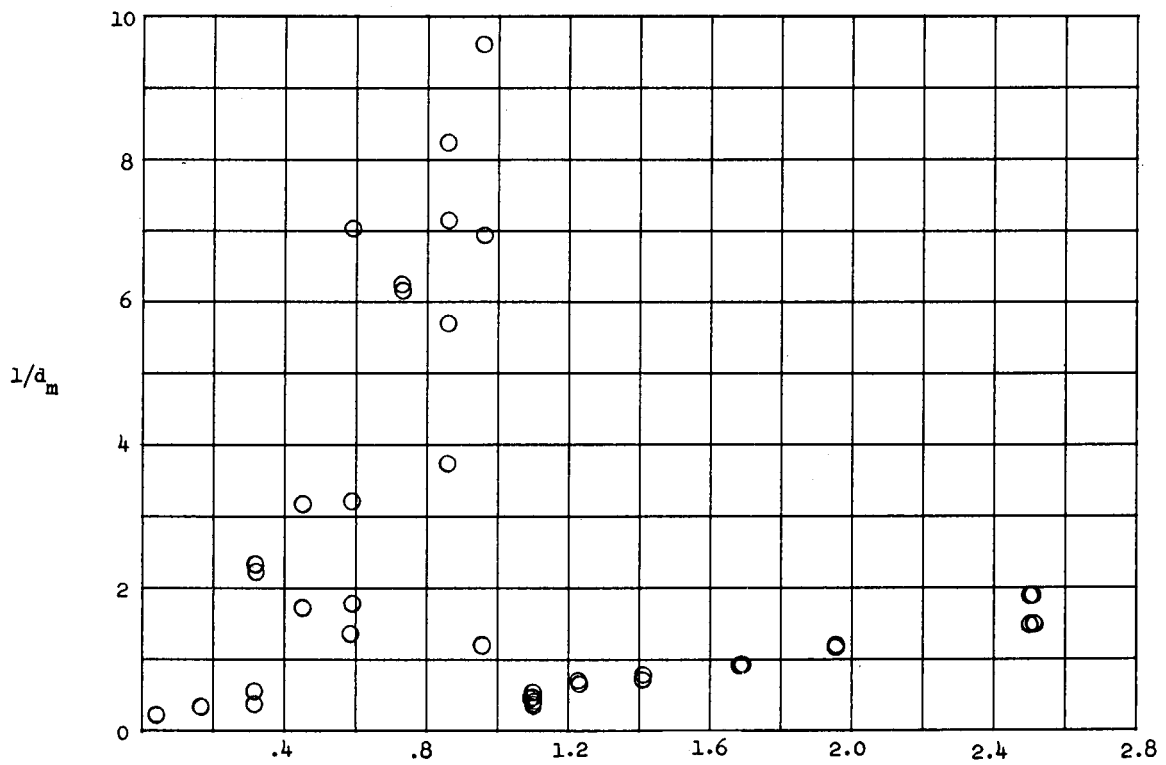


(b) Model 21; $d_m/d_j = 9.36$.

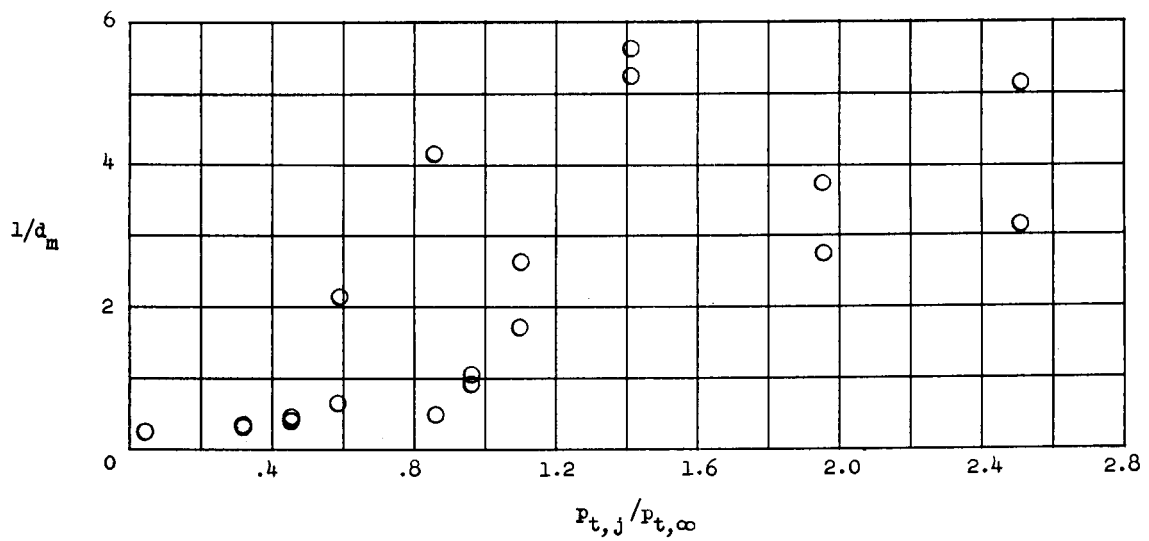


(c) Model 23; $d_m/d_j = 27.70$.

Figure 8.- Effect of ratio of jet total pressure to free-stream total pressure on main-stream shock-displacement distance for a nominal jet-exit Mach number of 3.0. $\alpha = 0^\circ$.

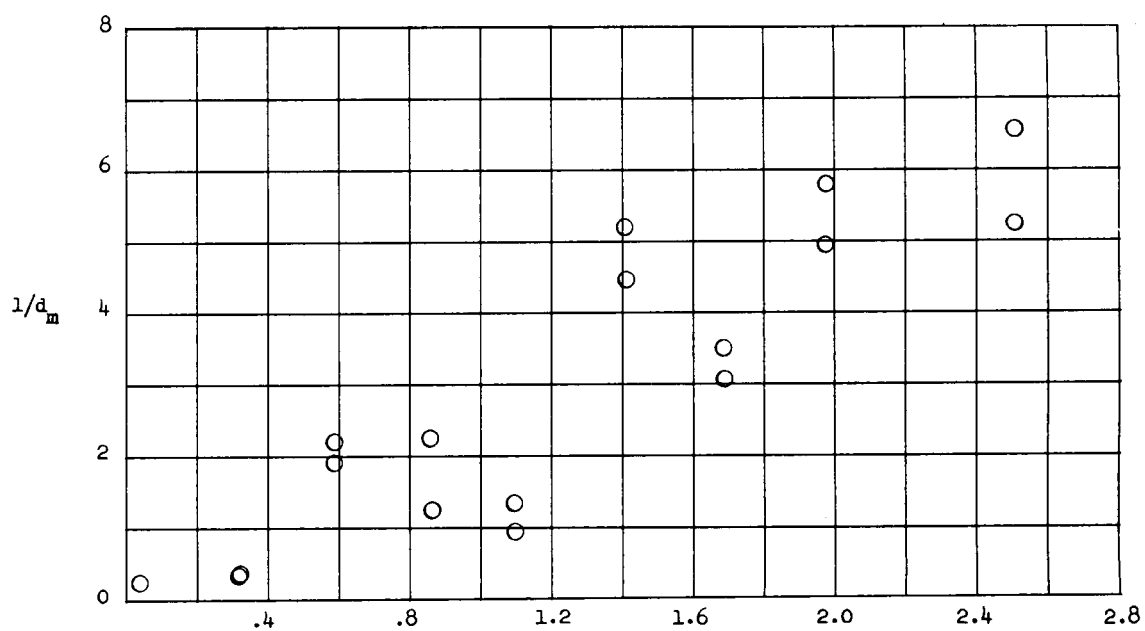


(a) Model 40; $d_m/d_j = 1.12$.

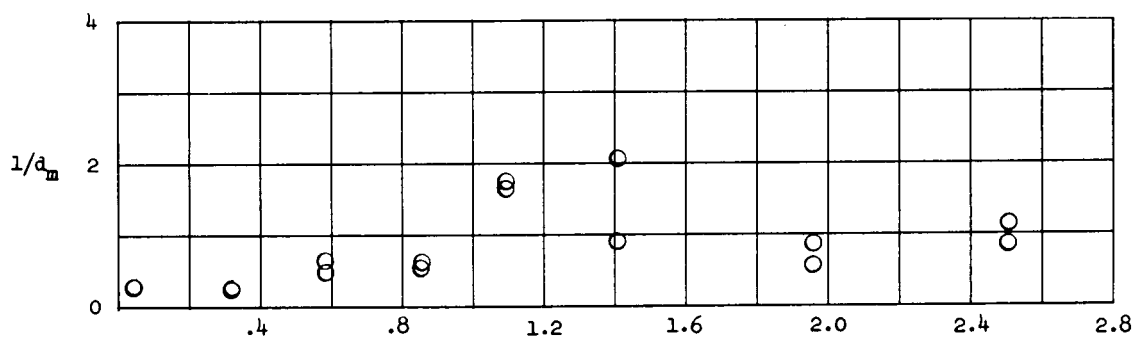


(b) Model 41; $d_m/d_j = 2.24$.

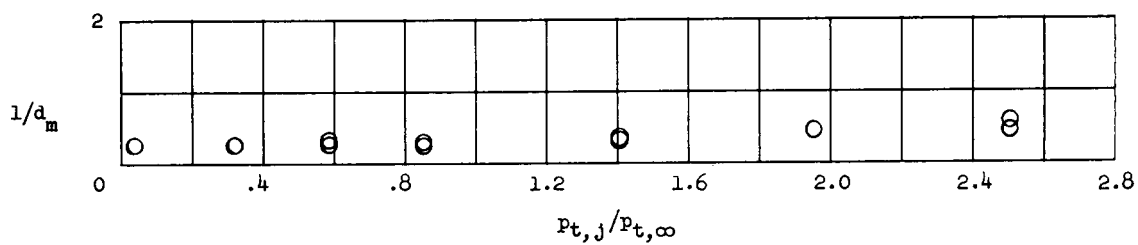
Figure 9.- Effect of ratio of jet total pressure to free-stream total pressure on main-stream shock-displacement distance for a nominal jet-exit Mach number of 6.4. Conical nozzle; $\alpha = 0^\circ$.



(c) Model 30; $d_m/d_j = 2.24$.

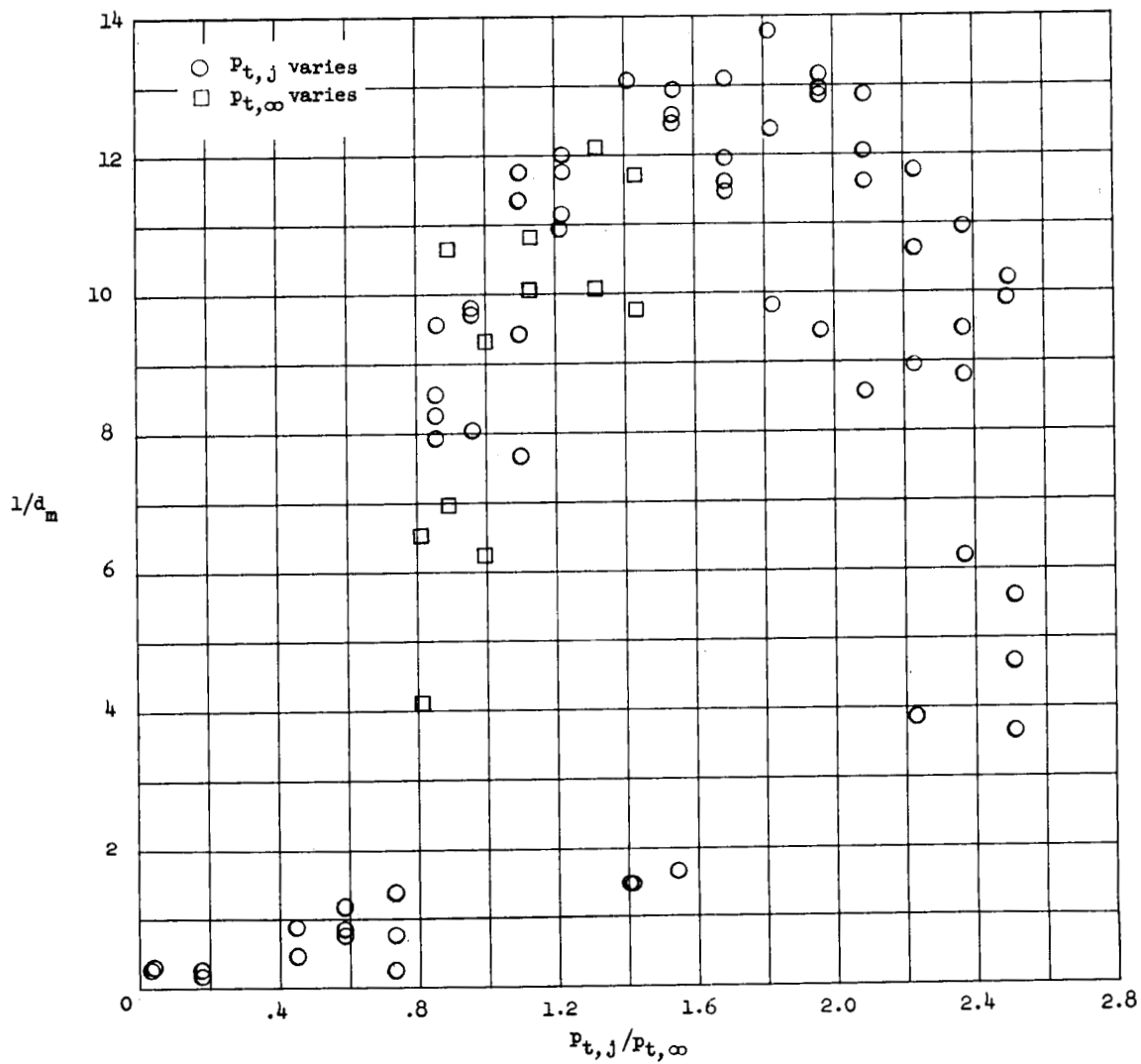


(d) Model 31; $d_m/d_j = 4.48$.



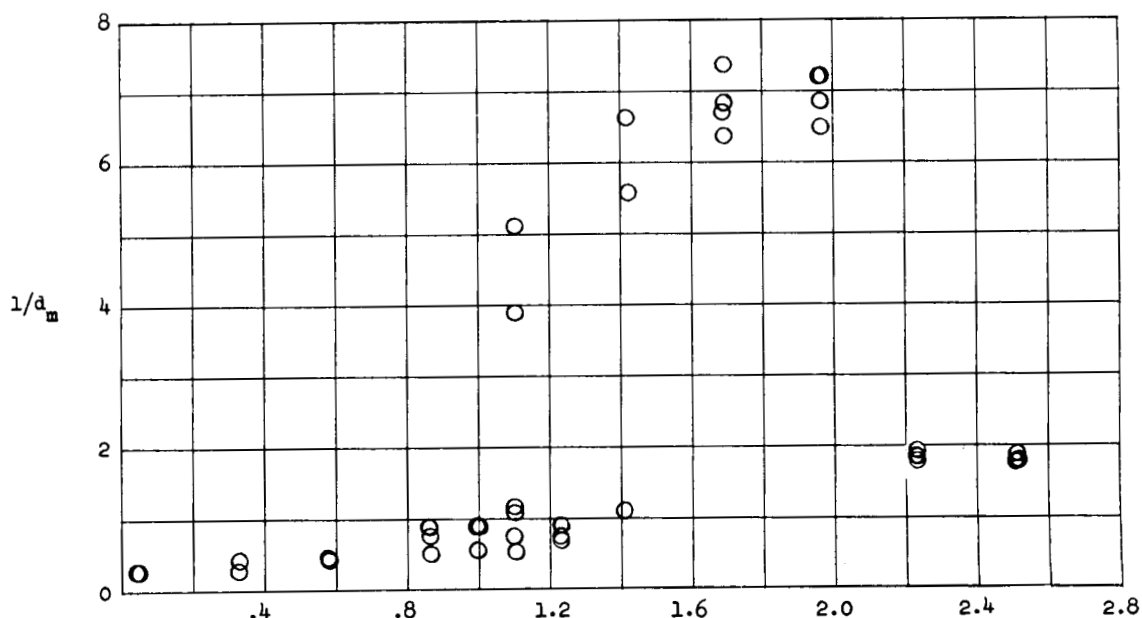
(e) Model 33; $d_m/d_j = 13.52$.

Figure 9.- Concluded.

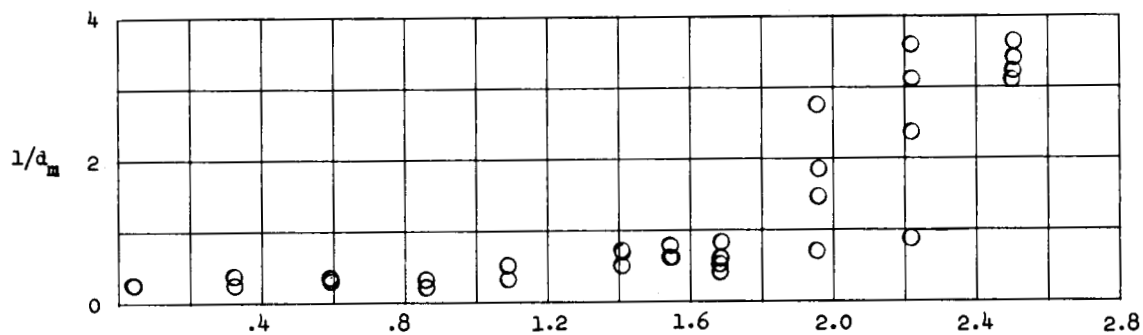


(a) Model 50; $d_m/d_j = 1.12$.

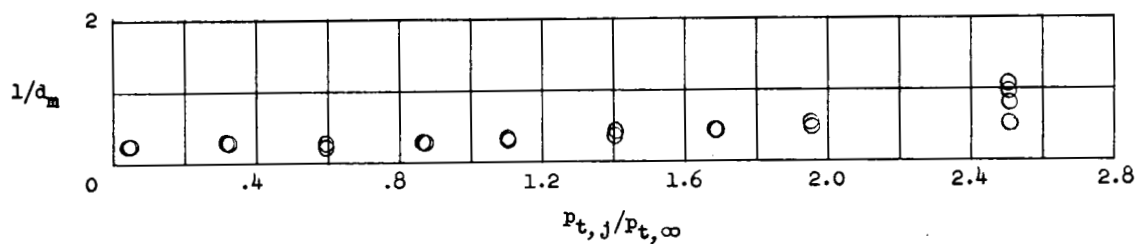
Figure 10.- Effect of ratio of jet total pressure to free-stream total pressure on main-stream shock-displacement distance for a nominal jet-exit Mach number of 6.4. Contoured nozzle; $\alpha = 0^\circ$.



(b) Model 51; $d_m/d_j = 2.24$.

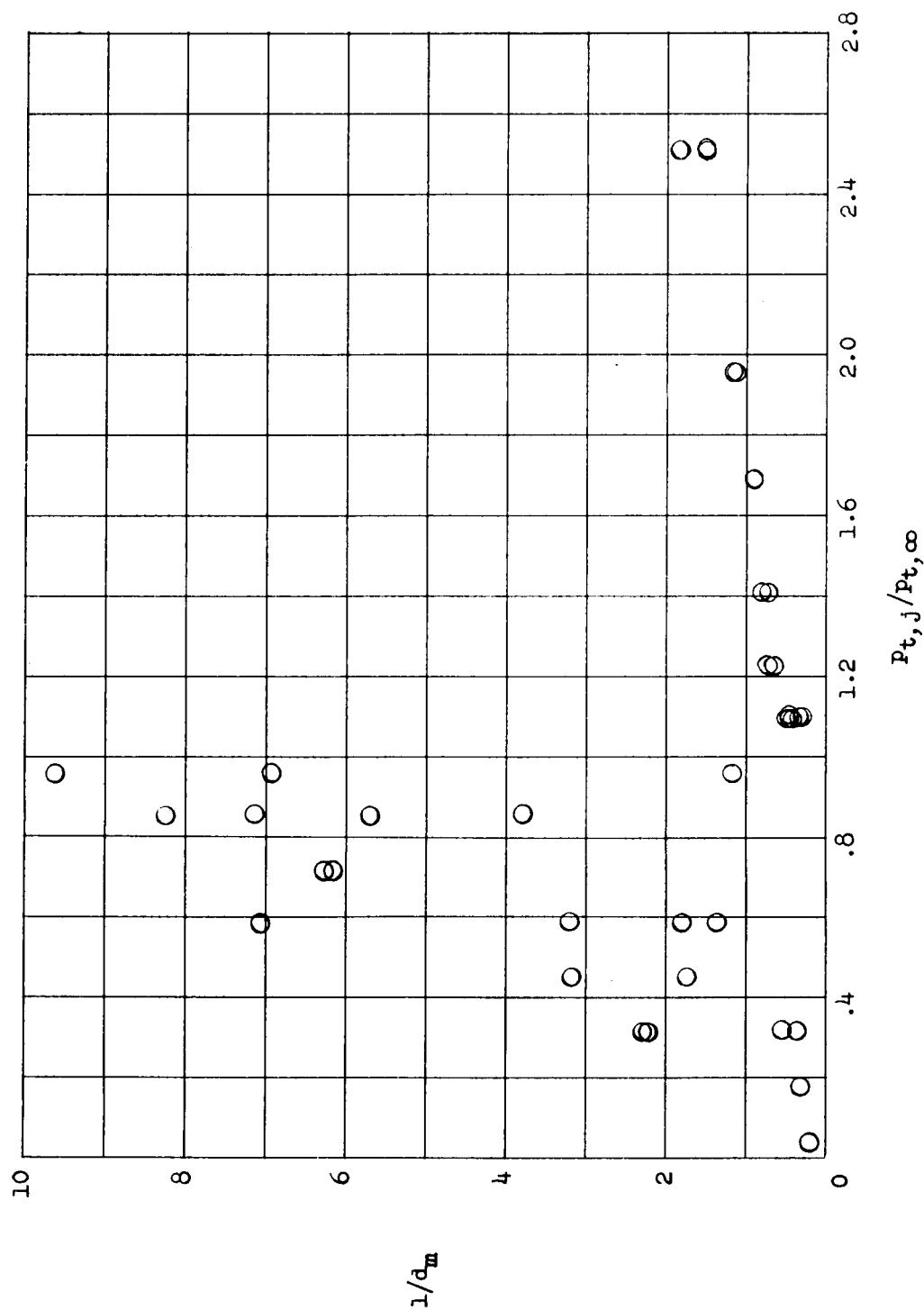


(c) Model 52; $d_m/d_j = 4.48$.



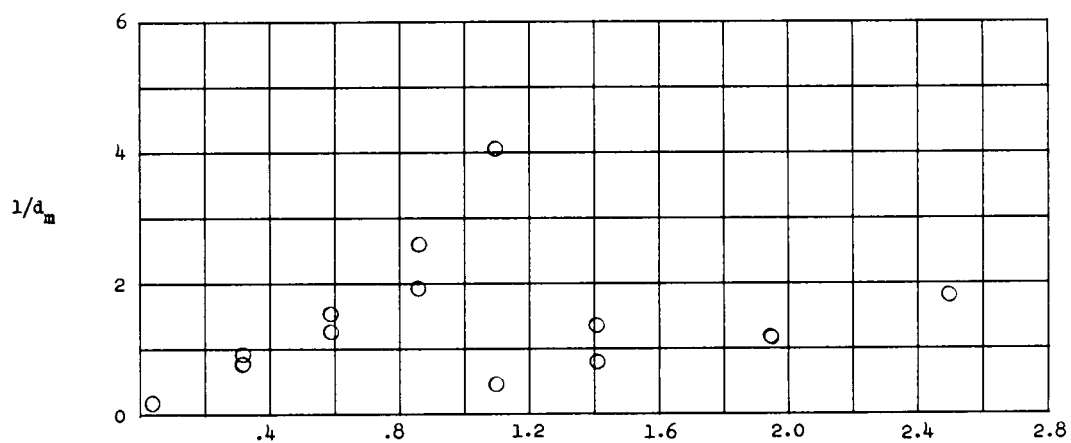
(d) Model 53; $d_m/d_j = 6.76$.

Figure 10.- Concluded.

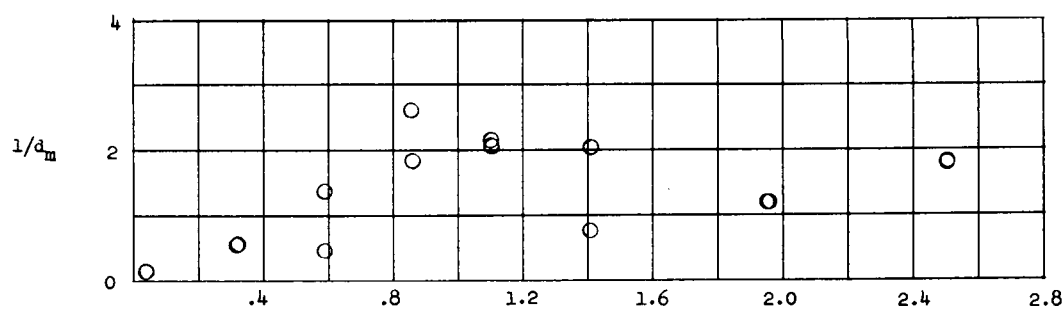


(a) $\alpha = 0^\circ$.

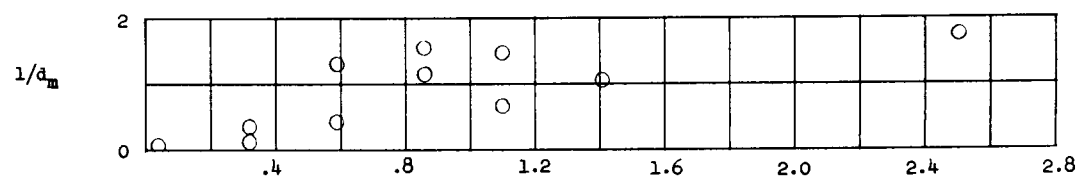
Figure 11.- Effects of ratio of jet total pressure to free-stream total pressure and angle of attack on main-stream shock-displacement distance for a nominal jet-exit Mach number of 6.4. Conical nozzle; model 40; $d_m/d_j = 1.12$.



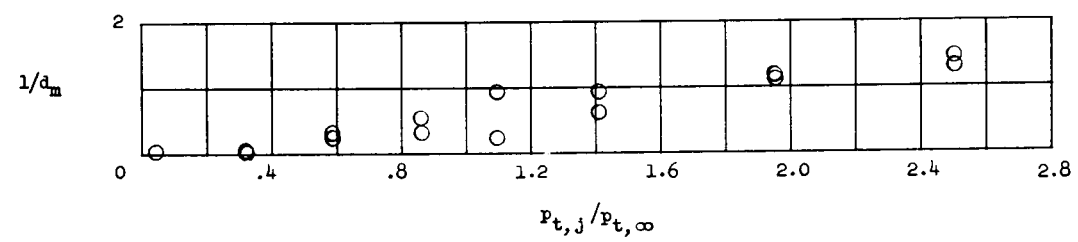
(b) $\alpha = 5^\circ$.



(c) $\alpha = 10^\circ$.

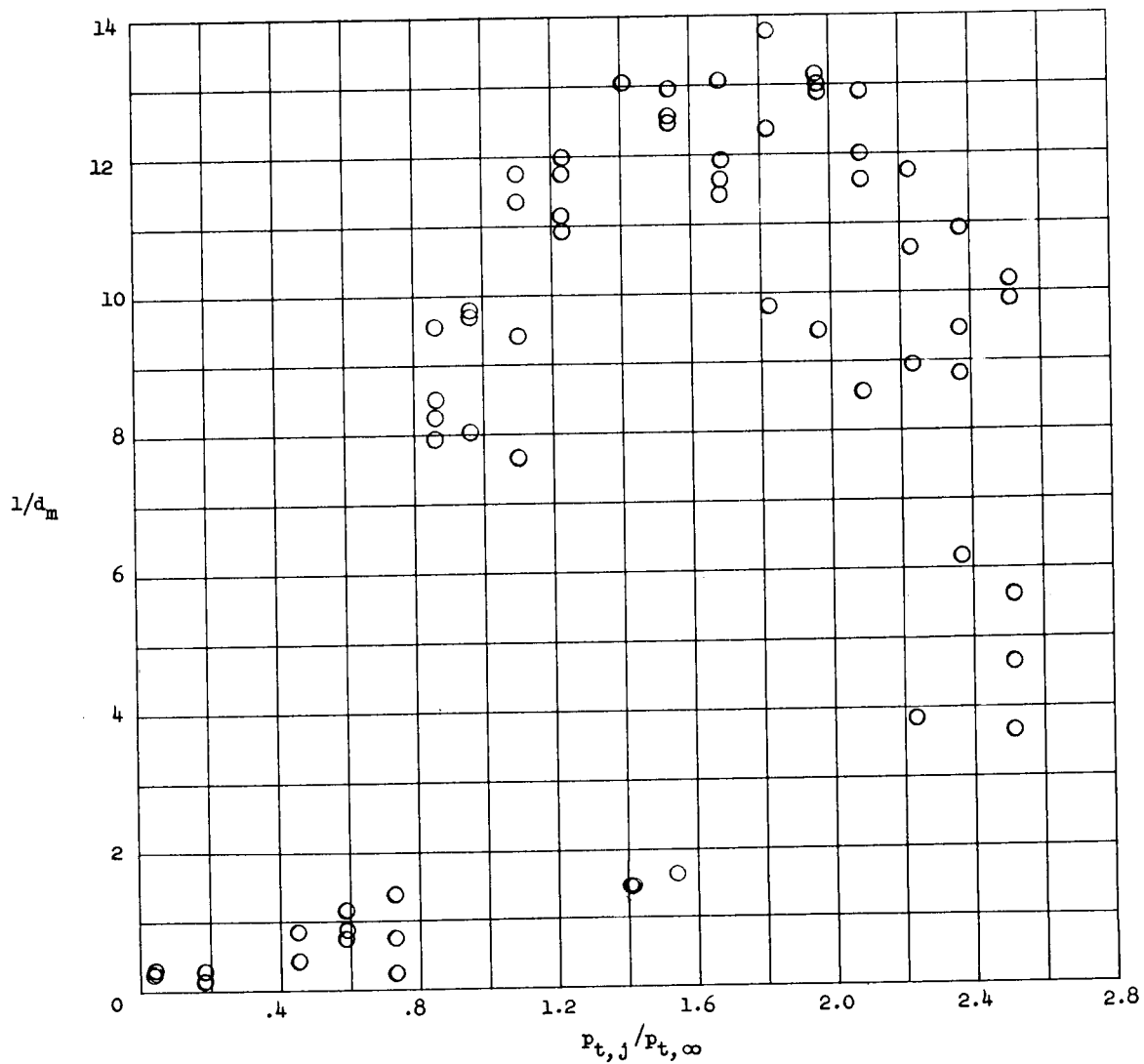


(d) $\alpha = 20^\circ$.



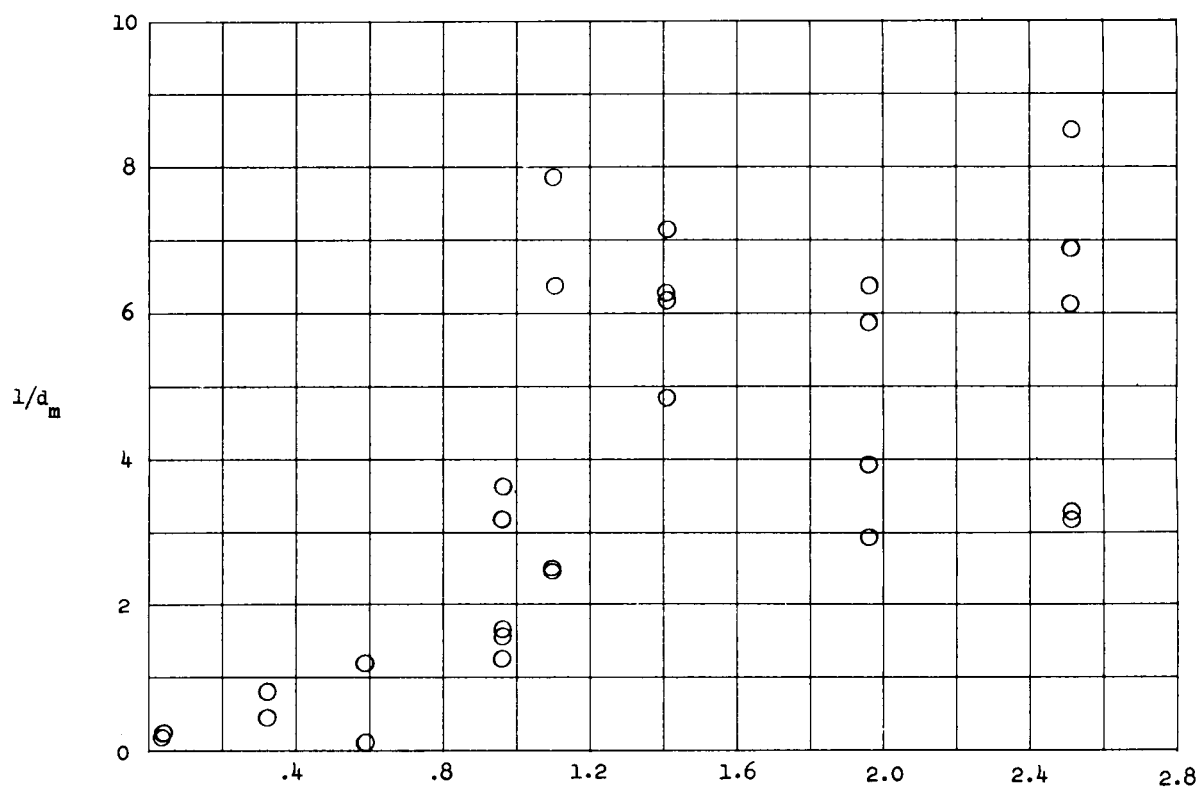
(e) $\alpha = 35^\circ$.

Figure 11.- Concluded.

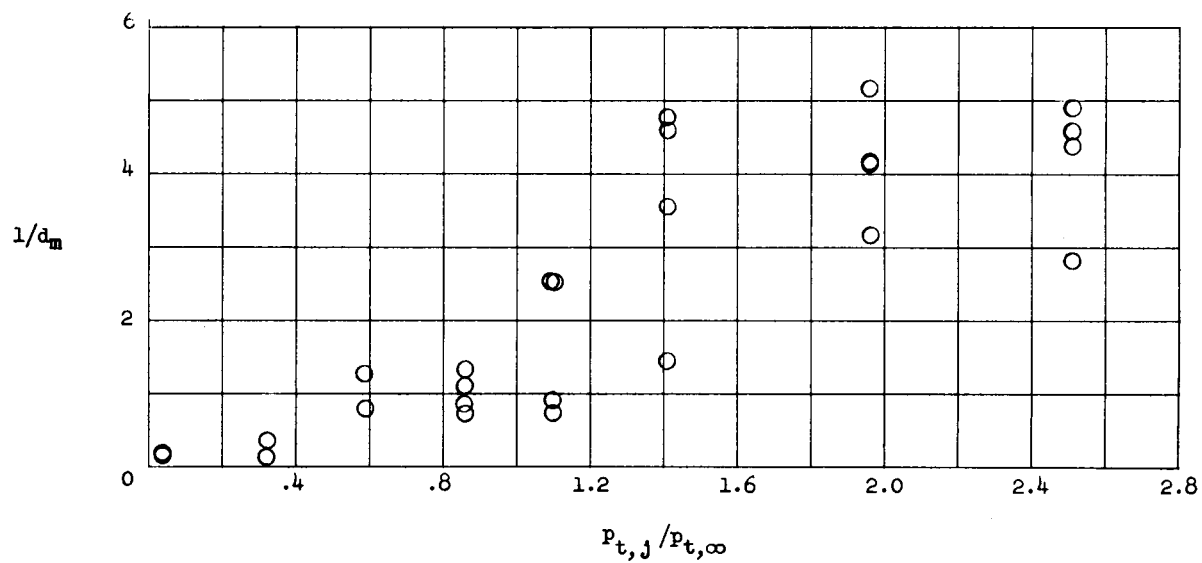


(a) $\alpha = 0^\circ$.

Figure 12.- Effects of ratio of jet total pressure to free-stream total pressure and angle of attack on main-stream shock-displacement distance for a nominal jet-exit Mach number of 6.4. Contoured nozzle; model 50; $d_m/d_j = 1.12$.

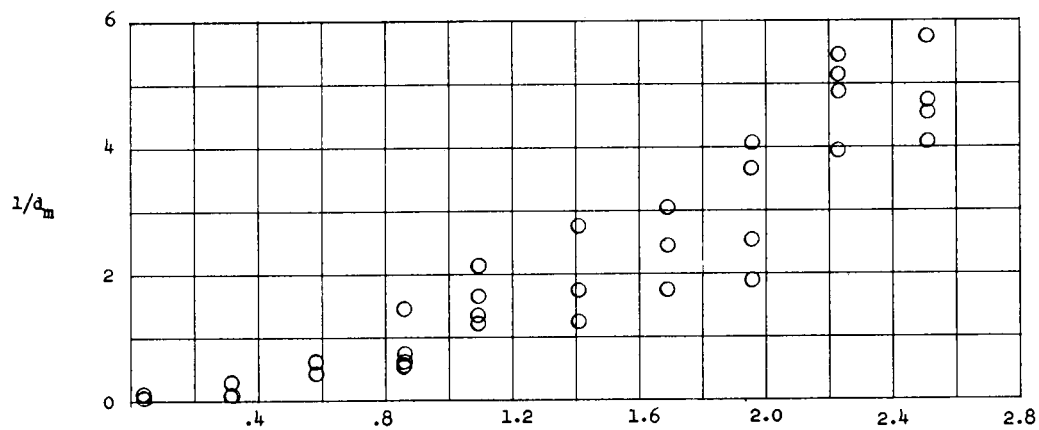


(b) $\alpha = 20^\circ$.

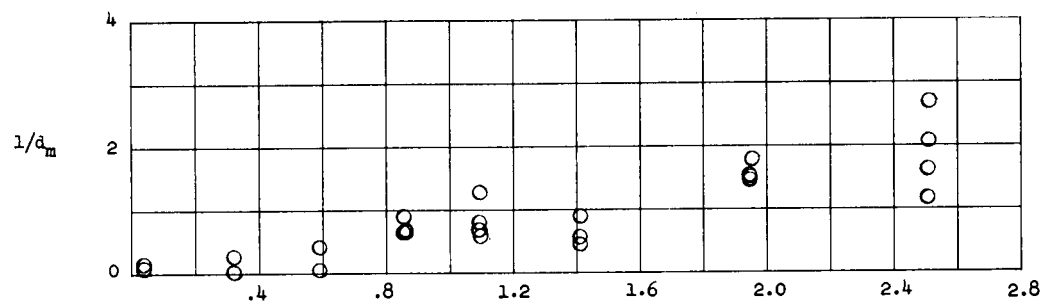


(c) $\alpha = 50^\circ$.

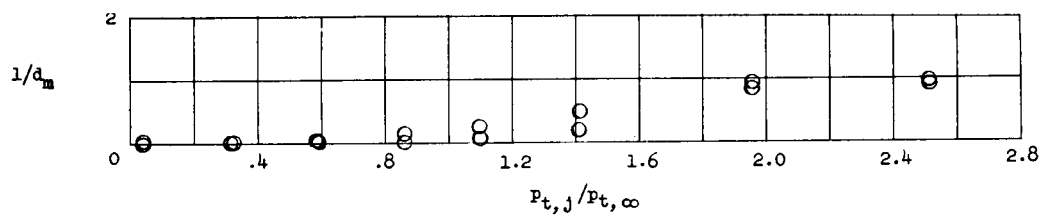
Figure 12.- Continued.



(d) $\alpha = 10^\circ$.

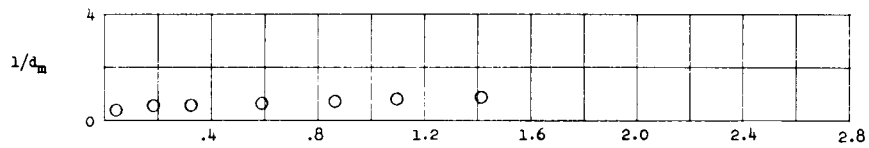


(e) $\alpha = 20^\circ$.

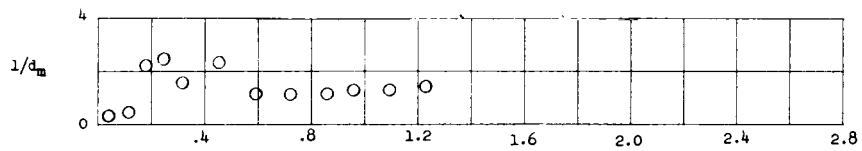


(f) $\alpha = 35^\circ$.

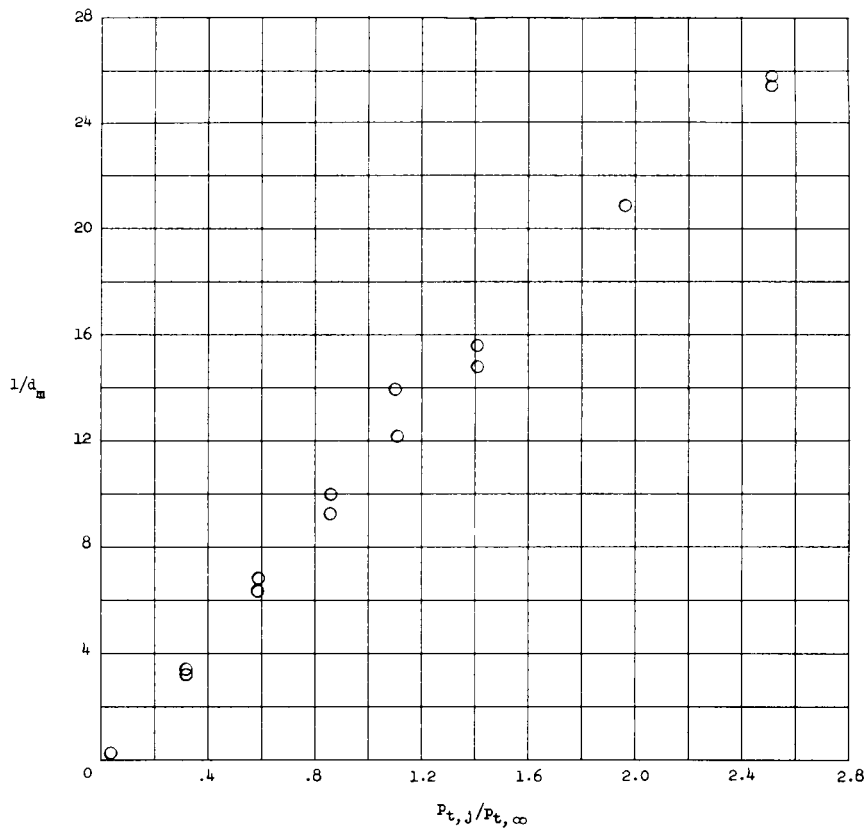
Figure 12.- Concluded.



(a) Model 14; $d_m/d_j = 9.62$; $M_j = 1.0$.

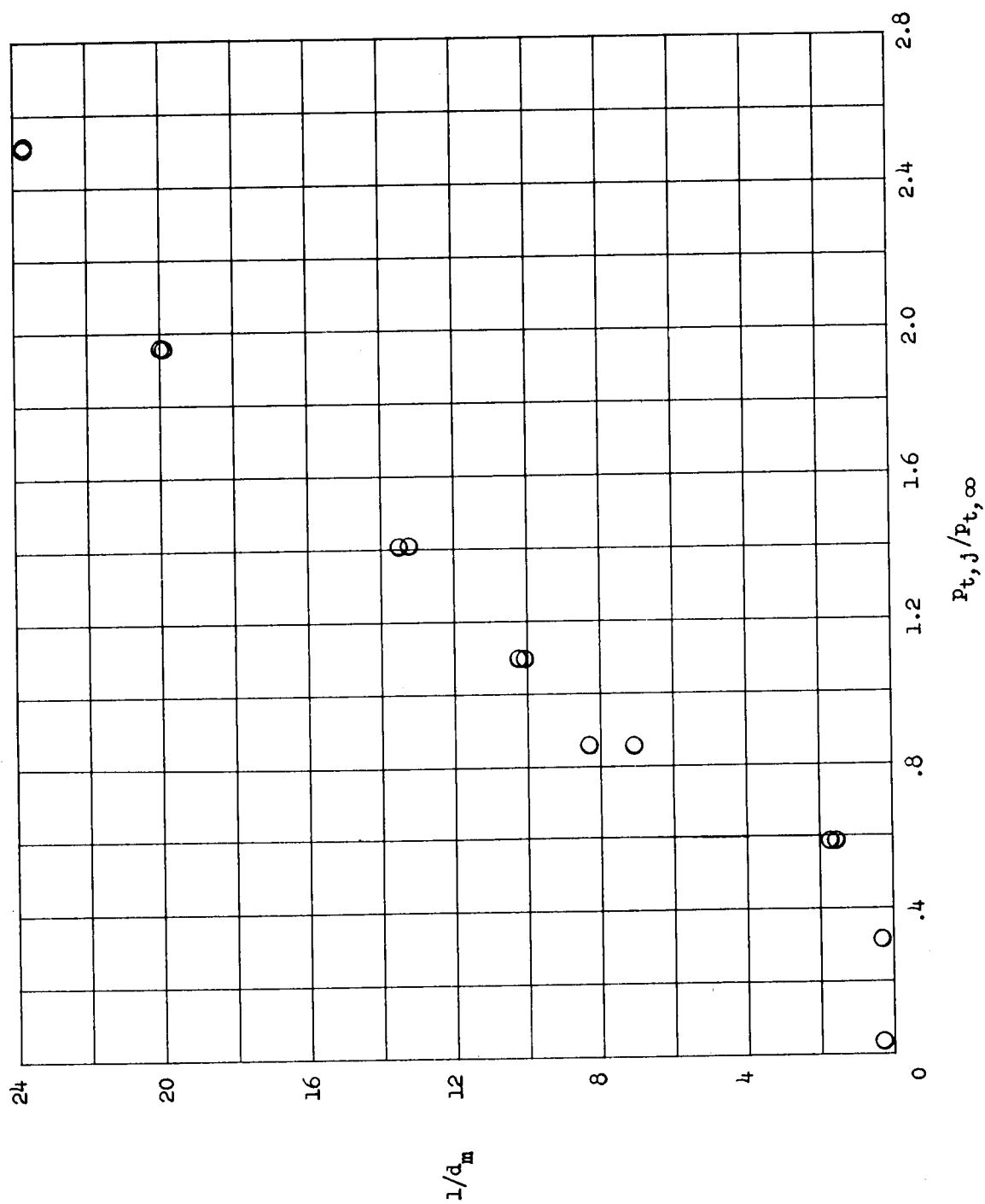


(b) Model 24; $d_m/d_j = 4.68$; $M_j = 3.53$.



(c) Model 44; $d_m/d_j = 1.12$; $M_j = 10.3$.

Figure 13.- Effect of ratio of jet total pressure to free-stream total pressure on main-stream shock-displacement distance for the tests which were conducted with helium. $\alpha = 0^\circ$.



(d) Model 54; $d_m/d_j = 1.12$; $M_j = 10.3$.

Figure 13.- Concluded.

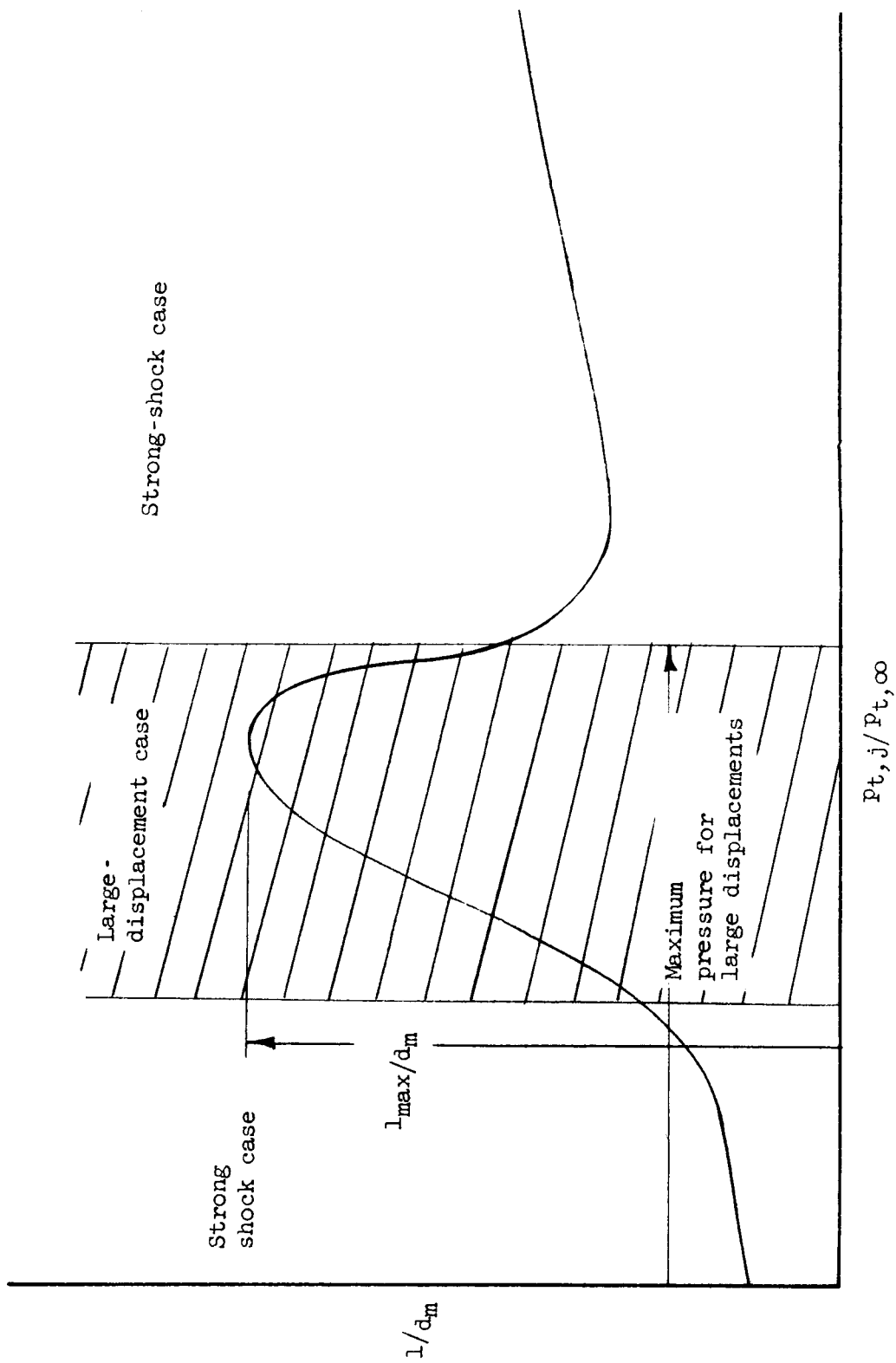


Figure 14.- Features of data interpretation.

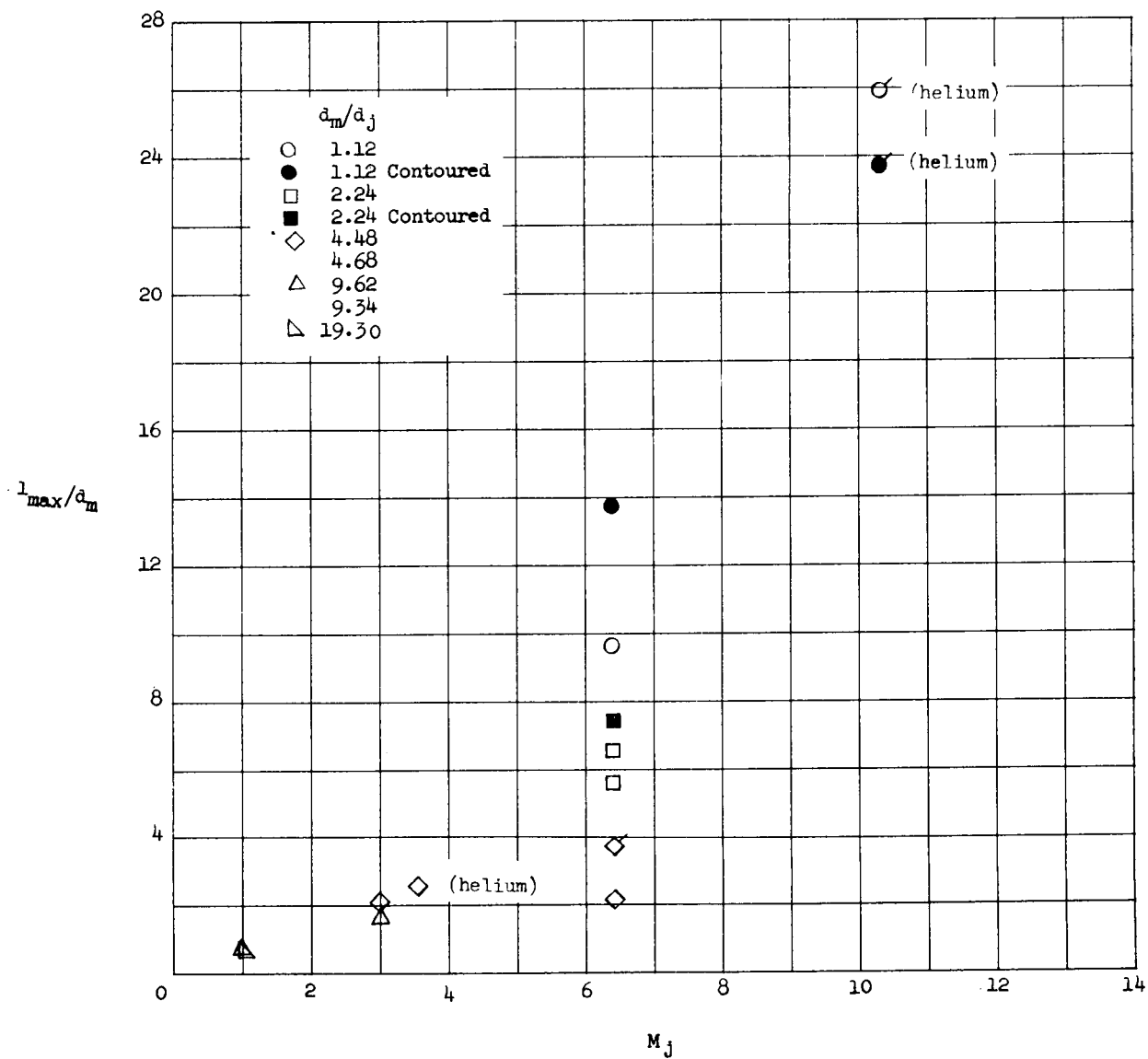


Figure 15.- Effect of jet-exit Mach number on the maximum main-stream shock-displacement distance. $\alpha = 0^\circ$. Flagged symbol indicates value may not have reached its maximum. Use of helium is indicated in parenthesis after test point.

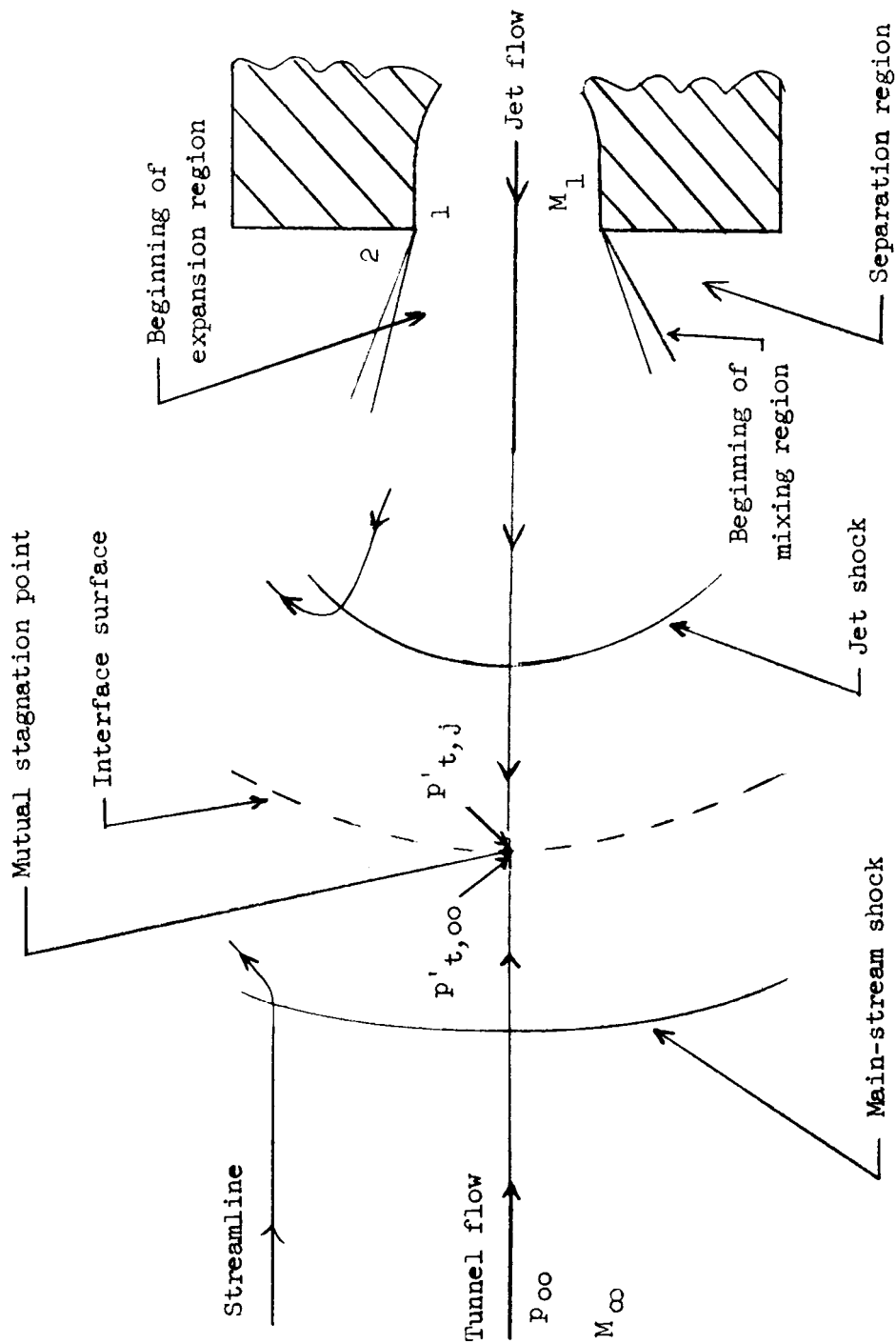
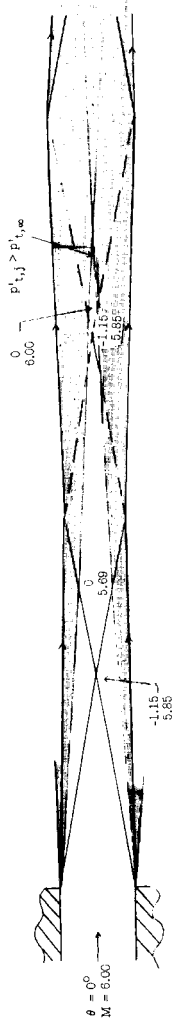
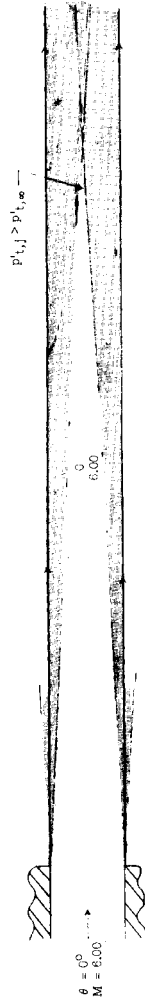


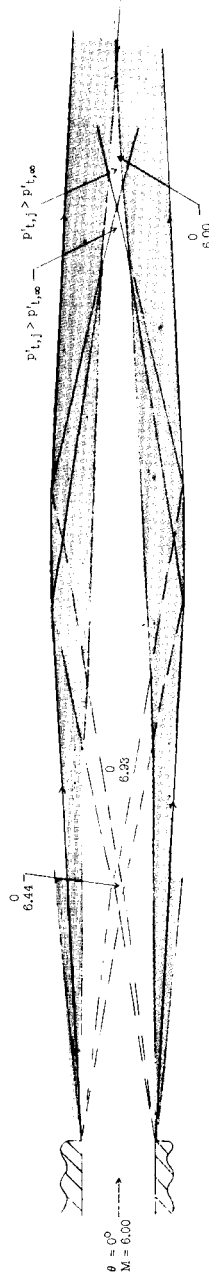
Figure 16.- Sketch of flow for strong-shock case.



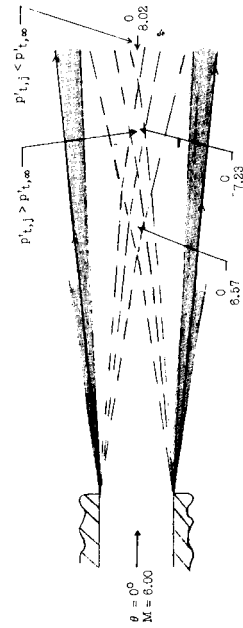
(a) Type of flow which corresponds to large-displacement case (normal-shock loss before mixing not sufficient for total-pressure loss); $P_1/P_2 = 0.85$ when $P_{t,j}/P_{t,\infty} = 1.1$.



(b) Type of flow which corresponds to large-displacement case (normal-shock loss before mixing not sufficient for total-pressure loss); $P_1/P_2 = 1.00$ when $P_{t,j}/P_{t,\infty} = 1.3$.



(c) Type of flow which corresponds to large-displacement case (normal-shock loss before mixing not sufficient for total-pressure loss); $P_1/P_2 = 1.54$ when $P_{t,j}/P_{t,\infty} = 2.00$.



(d) Type of flow which corresponds to strong-shock case (normal-shock loss before mixing sufficient for total-pressure loss); $P_1/P_2 = 2.30$ when $P_{t,j}/P_{t,\infty} = 3.00$.

Figure 17.- Illustrations of two types of shock displacements. P_2/P_∞ assumed to be 1.30 for $M_\infty = 6.00$; $M_j = 6.00$.

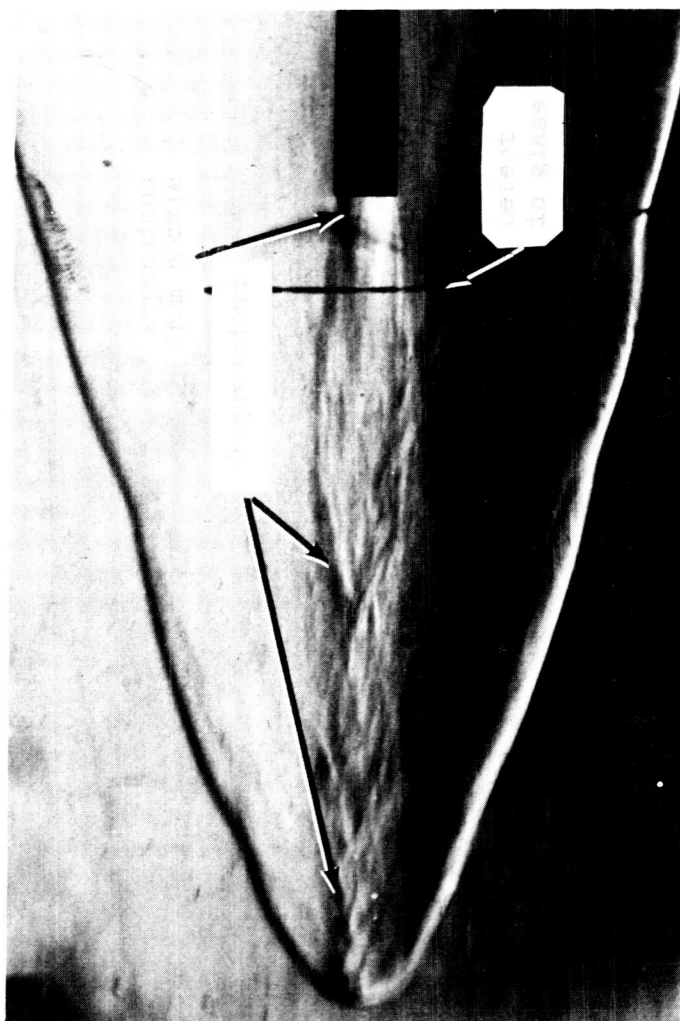


Figure 18.- Schlieren photograph of model 50 which illustrates patterns similar to figure 17(c). $p_{t,j}/p_{t,\infty} = 1.96$.
L-62-7042

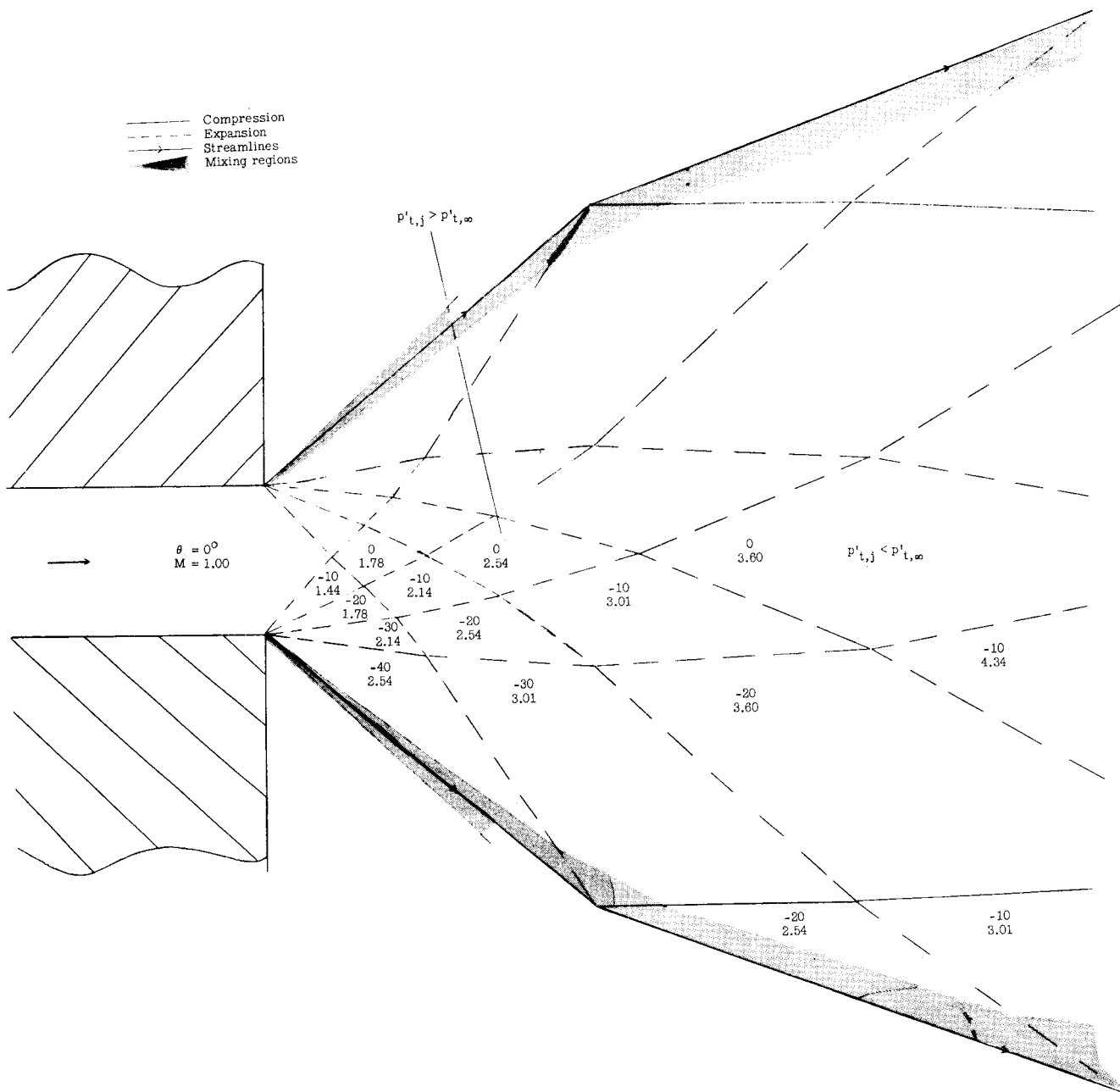
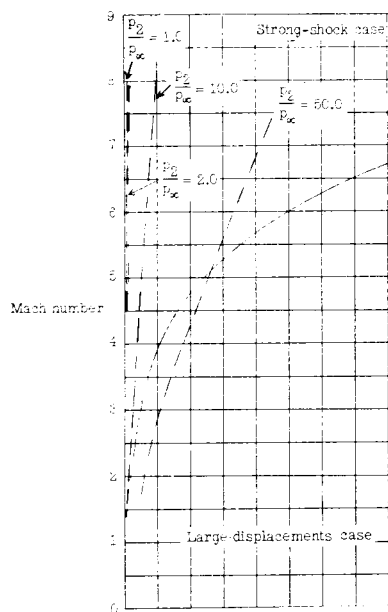
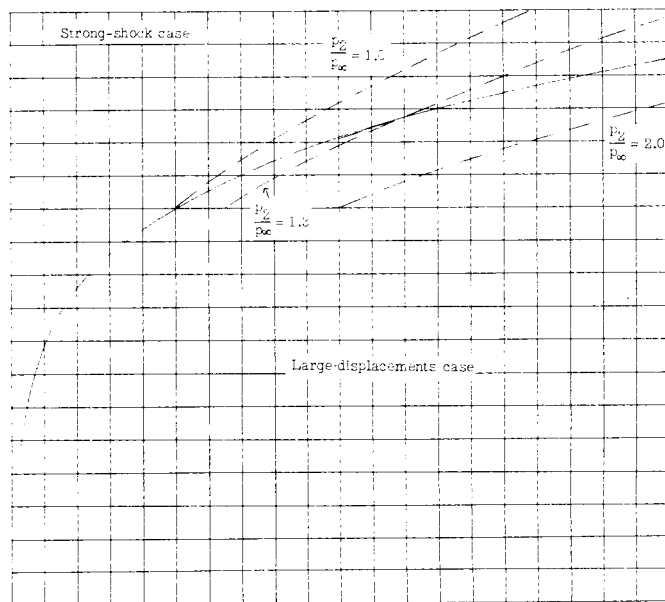


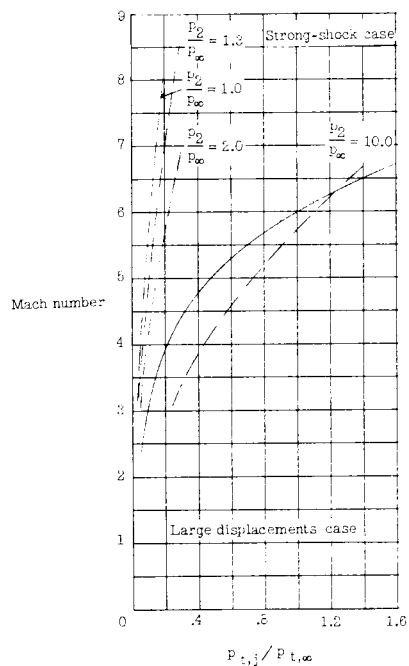
Figure 19.- Illustration of strong-shock case for a sonic jet nozzle. $p_1/p_2 = 9.56$ with p_2/p_∞ assumed to be 10; $M_\infty = 6.00$ and $p_{t,j}/p_{t,\infty} = 0.11$.



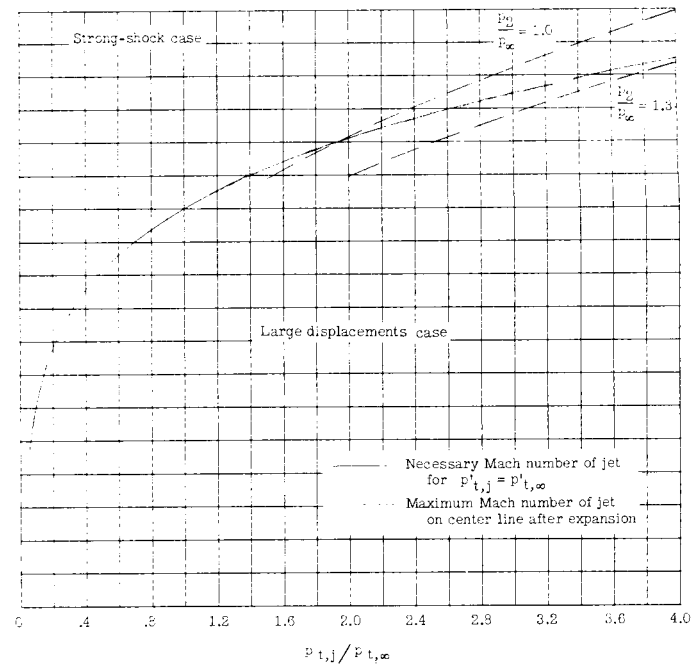
(a) $M_j = 1.0$.



(c) $M_j = 6.0$.

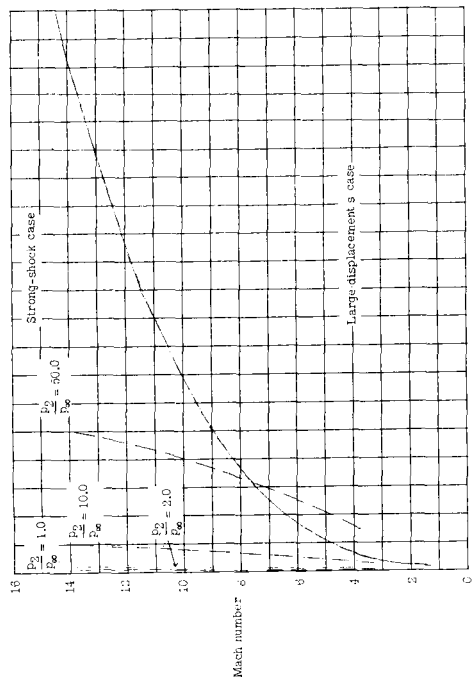


(b) $M_j = 3.0$.

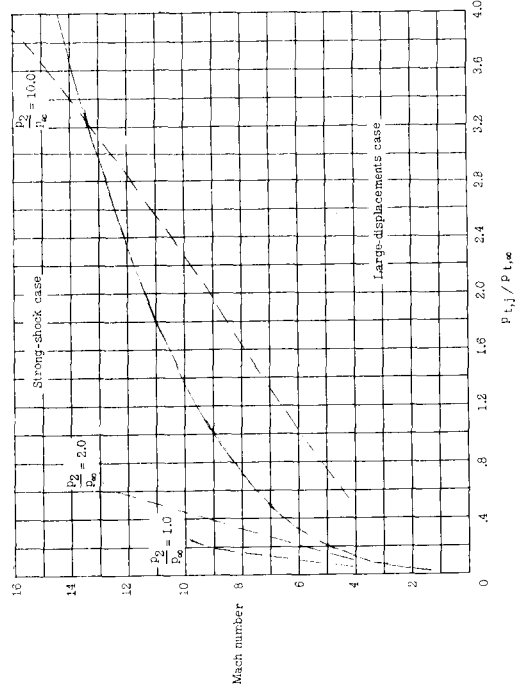


(d) $M_j = 6.40$.

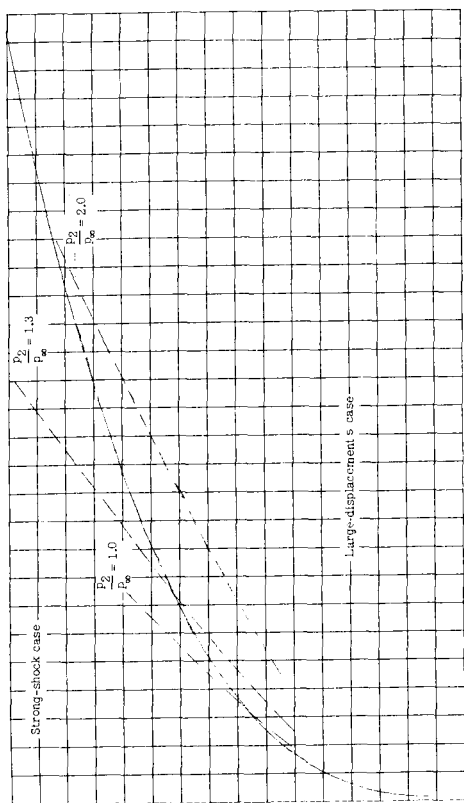
Figure 20.- Curves which illustrate possible regions for two types of shock displacements for different values of M_j . $\gamma = 1.40$; $M_\infty = 6.0$.



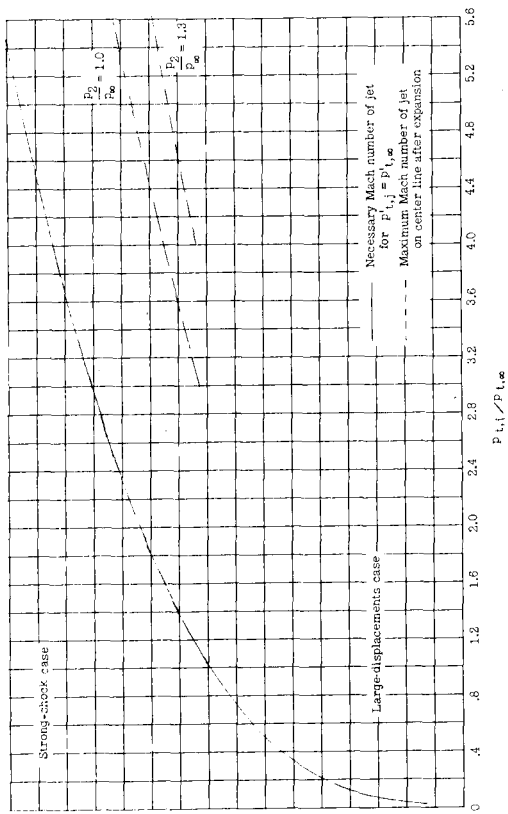
(a) $M_j = 1.0$.



(b) $M_j = 3.53$.

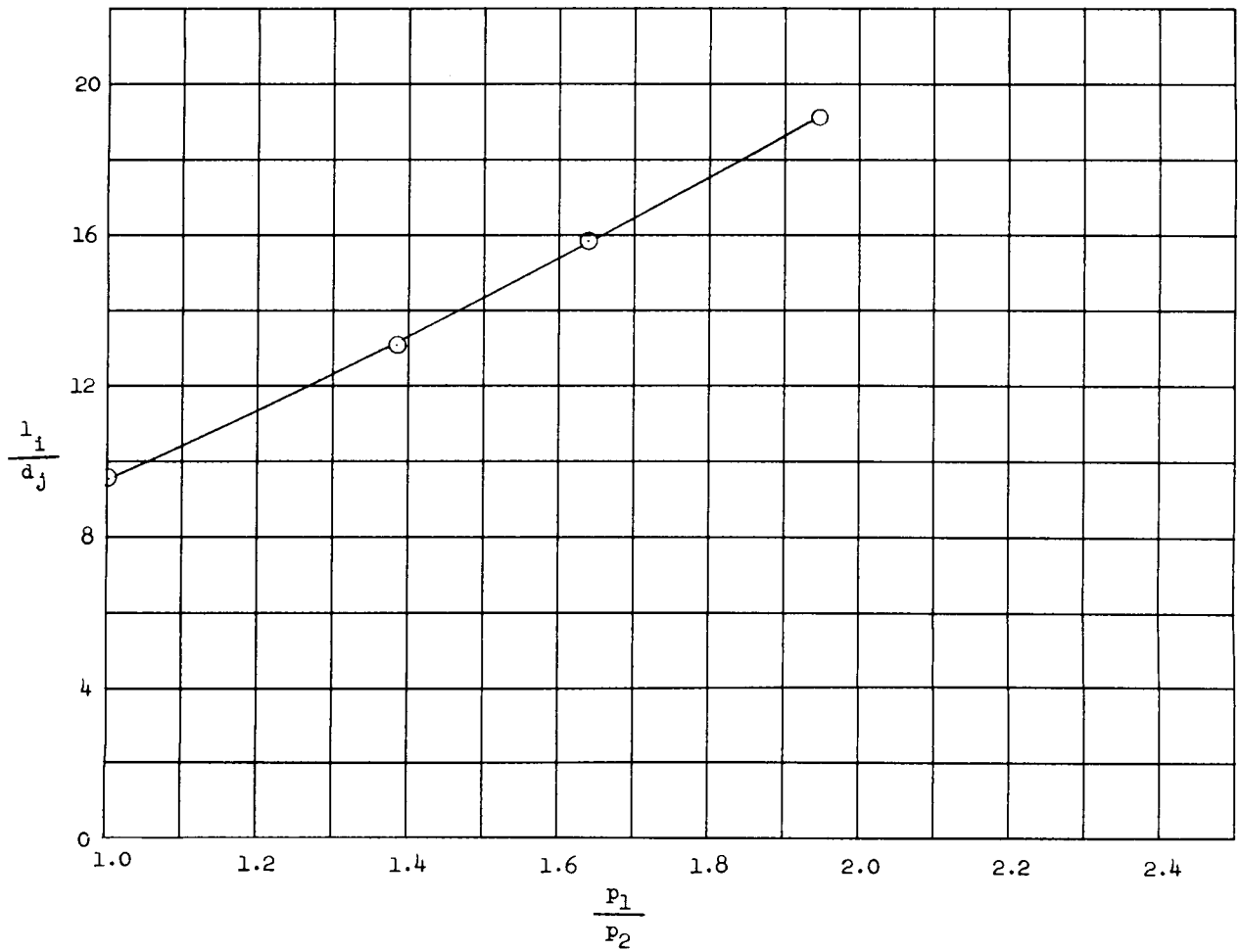


(c) $M_j = 6.0$.

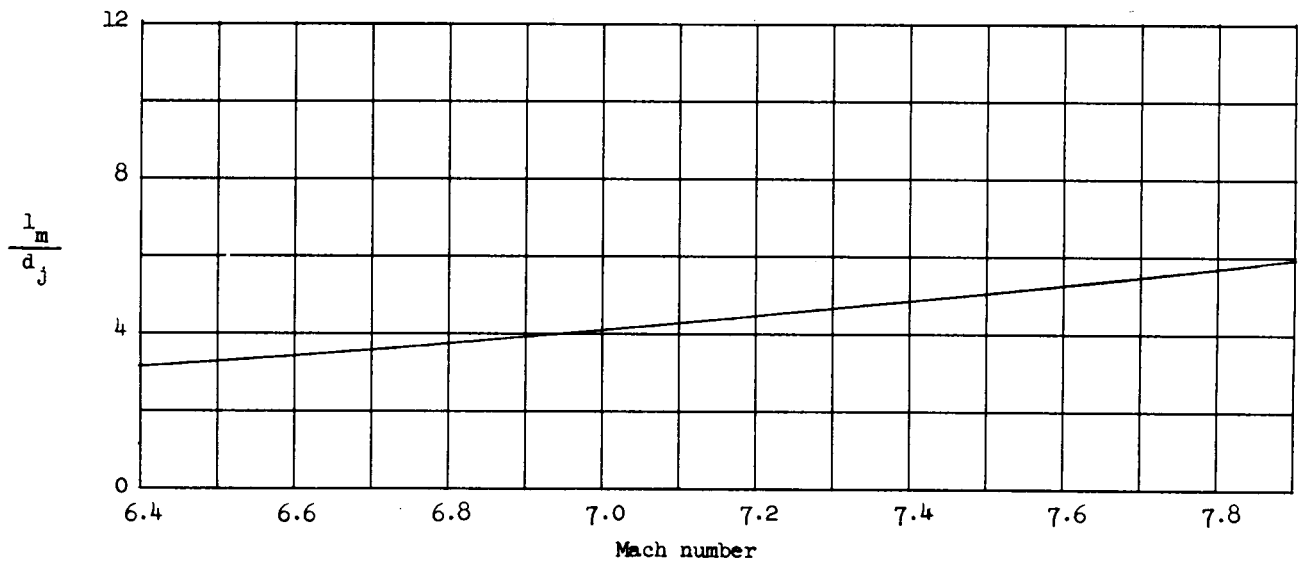


(d) $M_j = 9.26$.

Figure 21.- Curves which illustrate possible regions for two types of shock displacements for different values of M_j .
 $\gamma = 1.666$ (helium); $M_\infty = 6.0$.



(a) Distances from nozzle face to region where mixing boundaries overlap.



(b) Mach number along center line plotted against distance from nozzle face.

Figure 22.- Parameters obtained from two-dimensional characteristic layouts. $M_j = 6.4$.

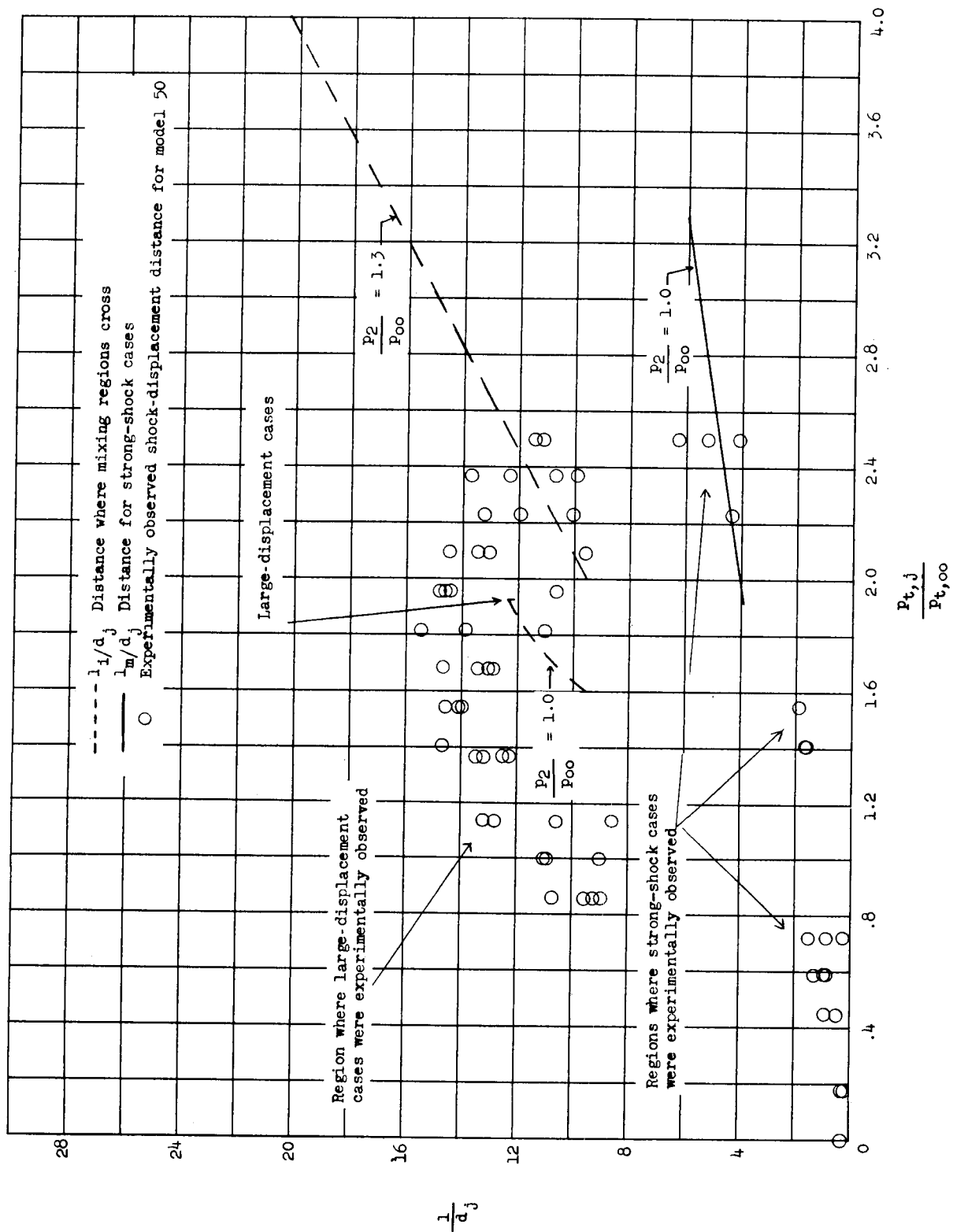


Figure 23.- Shock standoff distances calculated by using data from two-dimensional characteristic layouts for various free-stream pressures. $M_j = 6.4$; $M_\infty = 6.0$.